Benemérita Universidad Autónoma de Puebla

and

Dual C-P Institute of High Energy Physics, México

"Higgs physics at futures electron-proton colliders"

Speaker: Jaime Hernandez-Sanchez

LHeC and FCC-eh Collaboration

XXXVI Annual Meeting of the Division of Particles and Fields, September 2022

Outline

- The futures electron-proton colliders (LHeC, FCC-eh) and their goals.
- LHeC (FCC-he) vs. LHC, ee colliders and FCC-hh.
- Higgs physics BSM at LHeC and FCC-he.
- 2HDM-III as BSM: model with a four-zero Yukawa texture that controls the FCNC.
- Some interesting channels decays at tree level: H,h,A $\to$ bs,$\tau\mu$, H+ —> cb, ts, decays are sensitive to the pattern of Yukawa texture.
- We show the production e p$\to$q(h,H)ν_e with flavor violating decays of the Higgs bosons (h,H): cross sections, some distributions and cuts.
- We also present the production e- p —> q nu H-, considering H- —> c b

electrons for eh : ERL-e + FCC-hh [LHC]

- **Two 802 MHz Electron LINACs + 2x3 return arcs: using energy recovery in same structure: *sustainable* technology with power consumption < 100 MW** *instead of 1 GW for a conventional LINAC.*
- **Beam dump: no radioactive waste!**
- **high electron polarisation of 80-90%**

Concurrent eh and hh operation with same running time!

Genuine *Twin Collider* idea holds for LHC and FCC-hh.

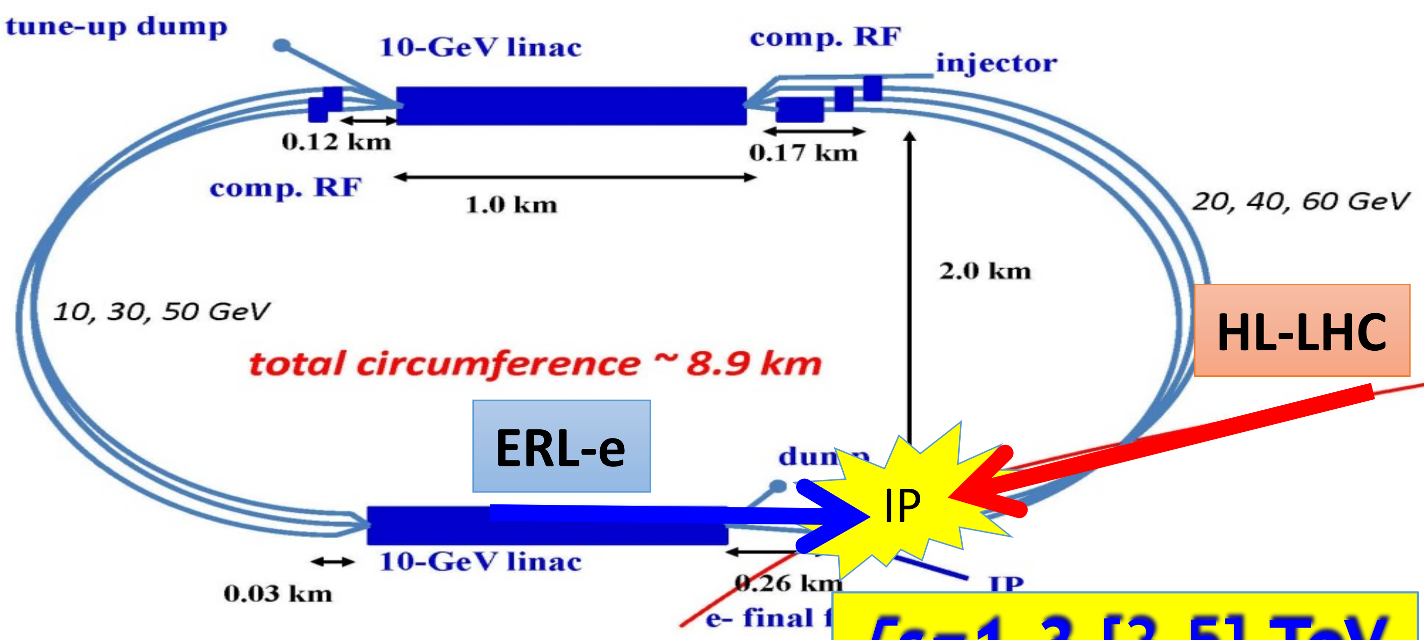

$\sqrt{s}$=1.3 [3.5] TeV
E_e = 60 GeV
E_p = 7 [50] TeV

- **ep peak lumi 10^{34} cm s^{-2} s^{-1}** (based on existing HL-LHC design)
- **Operation scenario: F. Bodry et al.** CERN-ACC-2018-0037 [arXiv:1810.13022]
- **LHeC** [FCC-eh] **L= 1000** [2000] **fb^{-1} total collected in 10** [20] **years**
- **'No' pile-up**: <0.1@LHeC; ~1@FCCeh

ERL design detailed in LHeC CDR: J. Phys. G: Nucl. Part. Phys. 39 (2012) 075001 [arXiv:1206.2913] and CDR update CERN-ACC-Note-2020-0002 [arXiv:2007.14491] and submitted to J. Phys. G → **see Talk #729 by B Holzer & Talk #730 about ERL Facility at Orsay**

Uta Klein, 29.07.22 (Talk at ICHEP 2020, Prague)

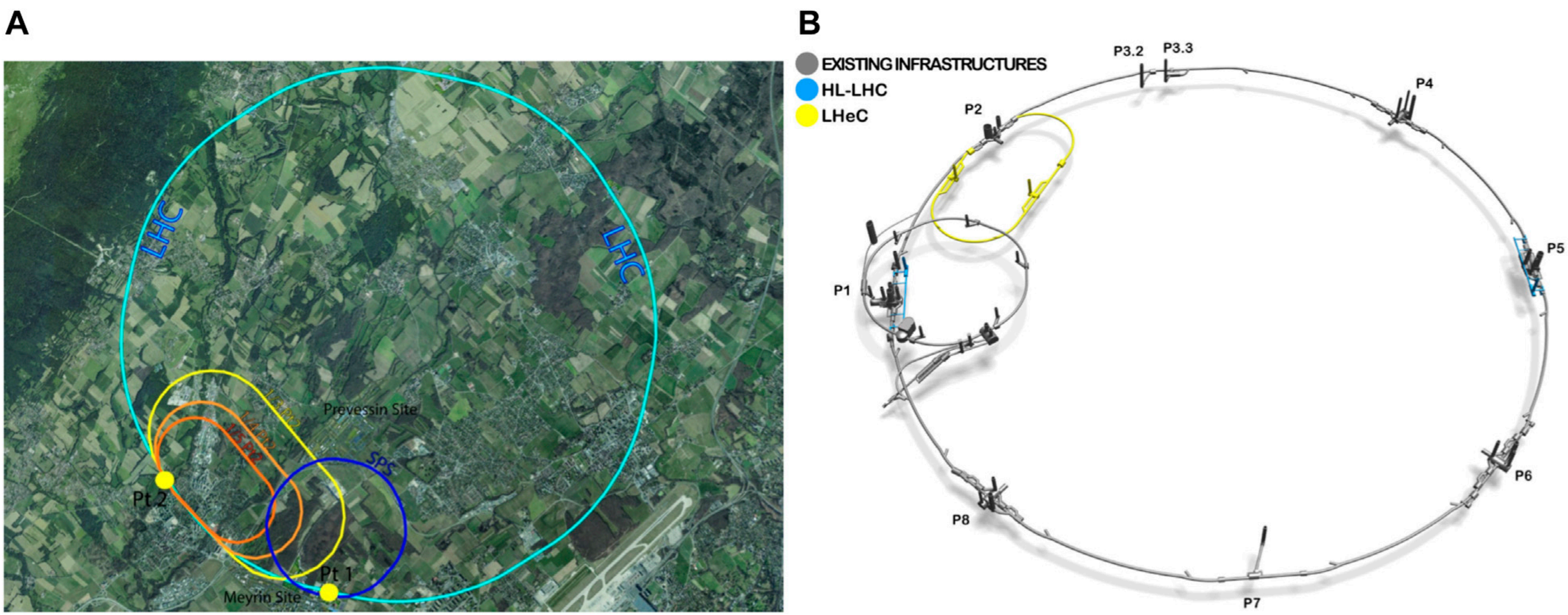

FIGURE 2 | (A) Layout options and footprint of the LHeC in the Geneva basin next to the Geneva airport and CERN. The yellow racetrack corresponds to the LHeC layout that offers optimal performance; in orange, two size variations explored for cost optimization. For reference, the light blue circle depicts the existing tunnel of the LHC; the dark blue circle is the SPS. **(B)** 3D schematic showing the underground tunnel arrangement. The grey sections indicate the existing SPS and LHC tunnel infrastructures and the yellow section the new LHeC installation.

This machine could be start around 2032

Brüning O, Seryi A and Verdú-Andrés S (2022) Electron- Hadron Colliders: EIC, LHeC and FCC- eh. Front. Phys. 10:886473.

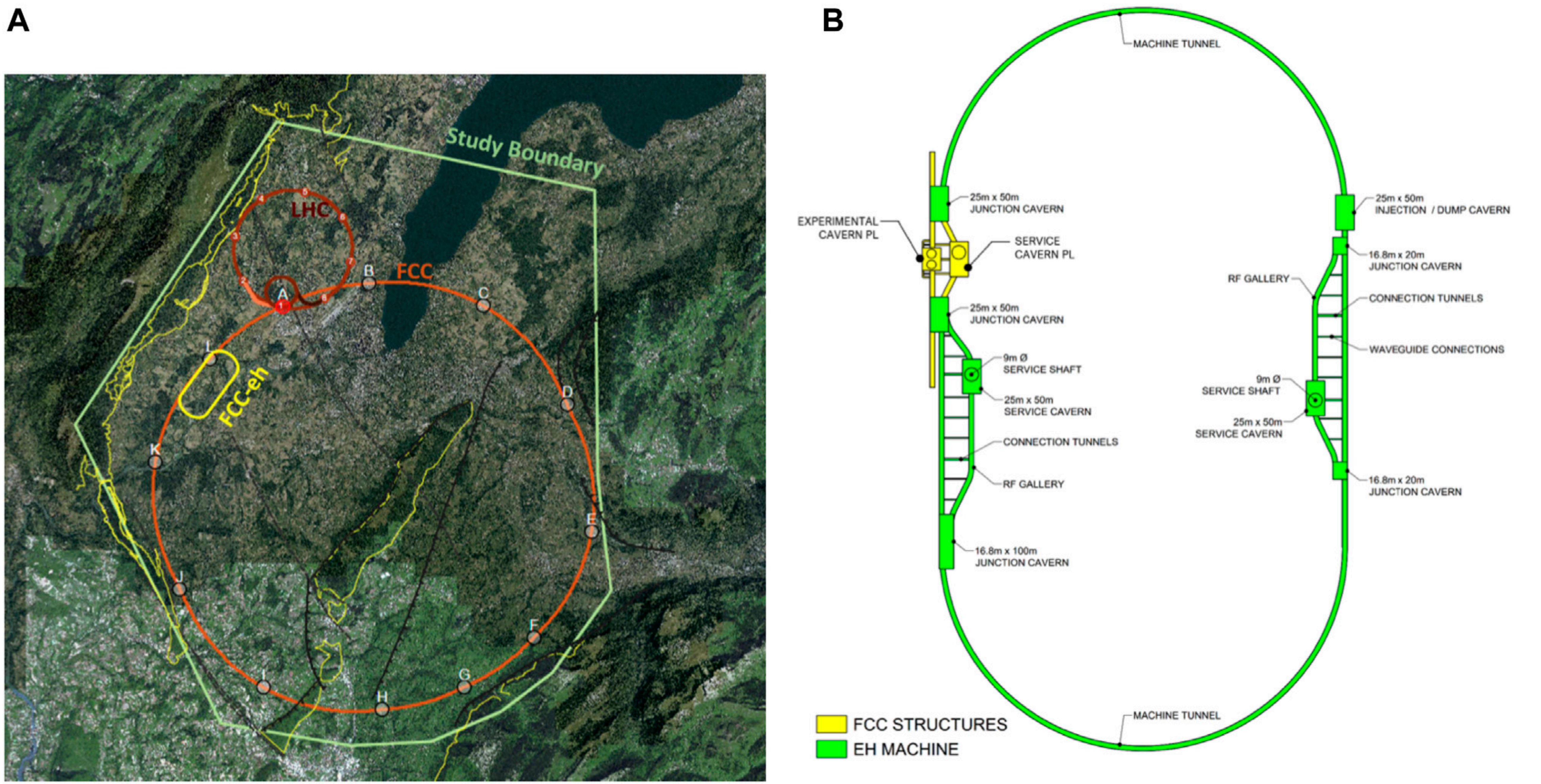

FIGURE 3 | FCC-eh layout and underground structures of the FCC-eh. **(A)** The FCC-eh layout next to the FCC and LHC infrastructures. The yellow lines indicate the ERL of the FCC-eh, the light red lines the FCC installation and the dark red the existing LHC tunnel. **(B)** Schematic layout of the ERL underground structures for the FCC-eh.

FCC-ee could be start around 2037/2045
FCC-hh around 2070's
FCC Collaboration CDR Volumen 1-4

SM Higgs Production in ep

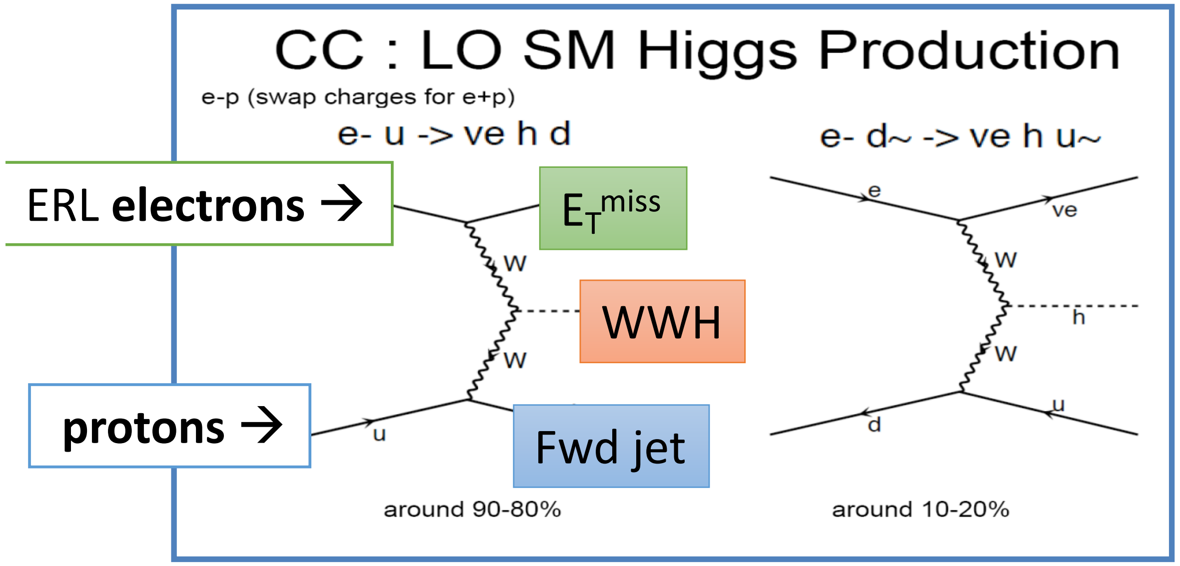

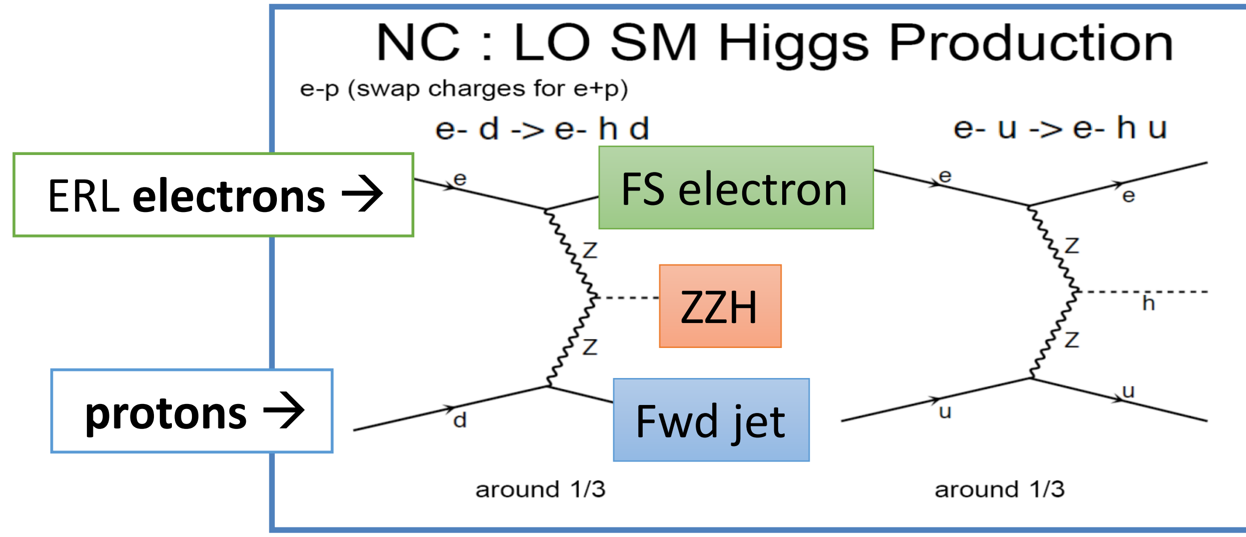

→ In ep, direction of quark (FS) is well defined.

Total cross section [fb]
(LO QCD CTEQ6L1 M_H=125 GeV)

c.m.s. energy	1.3 TeV LHeC	3.5 TeV FCC-eh
CC DIS NC DIS	109 21	560 127
P=-80% CC DIS NC DIS	 **196** **25**	 **1008** **148**

- Scale dependencies of the LO calculations are in the range of 5-10%. Tests done with MG5 and CompHep.
- **NLO QCD corrections are small**, but shape distortions of kinematic distributions up to 20%. QED corrections up to -5%.

[J. Blumlein, G.J. van Oldenborgh , R. Ruckl, Nucl.Phys.B395:35-59,1993]
[B.Jager, arXiv:1001.3789]

Signal

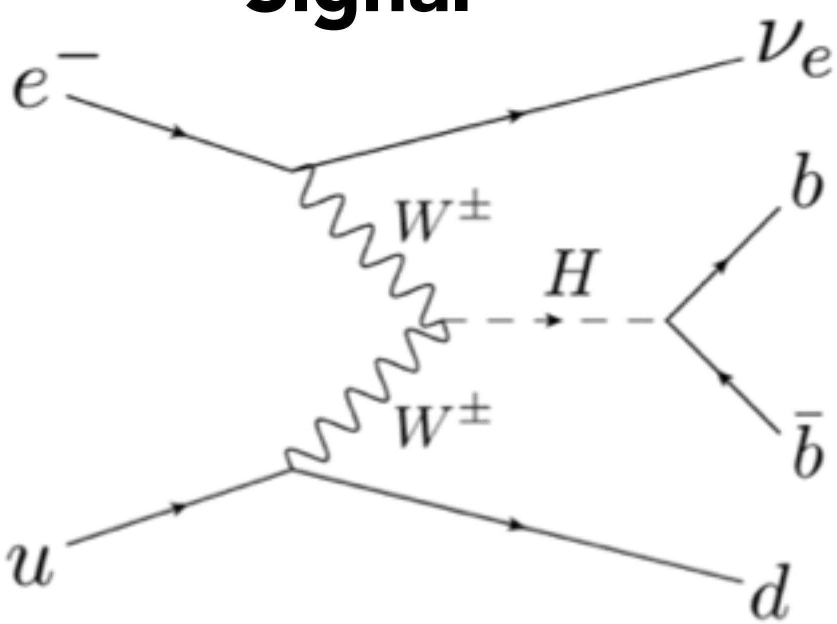

Charged current (CC) H->bb (0.063 pb)

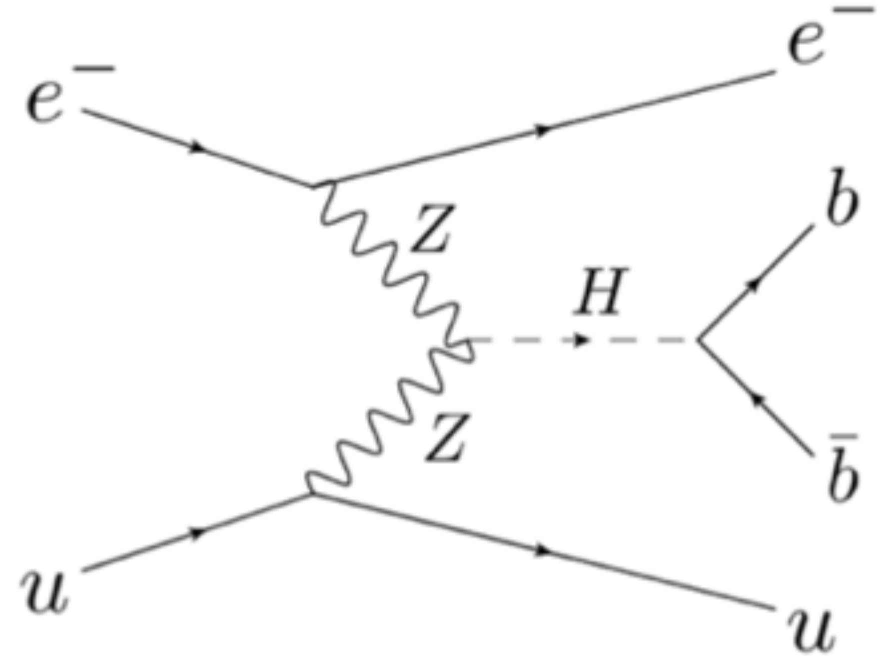

Neutral current (NC) H->bb (0.012 pb)

- CC: H->bb process is chosen as the signal because the cross section is larger than NC: H->bb process and NC rejection cut decreases large number of NC BG.

Background

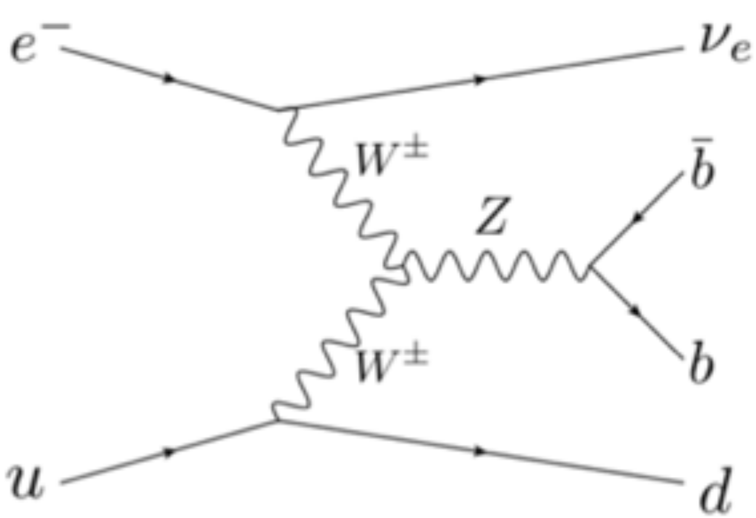

CC Z production (0.29 pb)

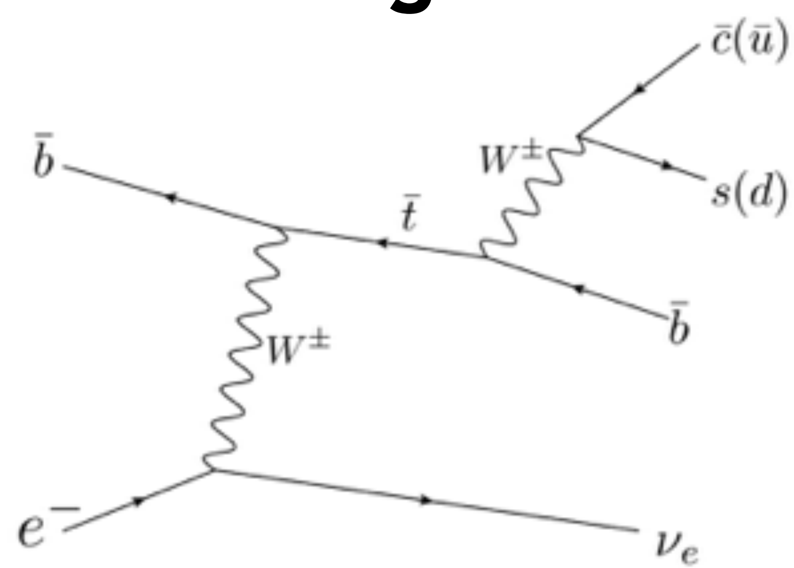

Single top production (0.43 pb)

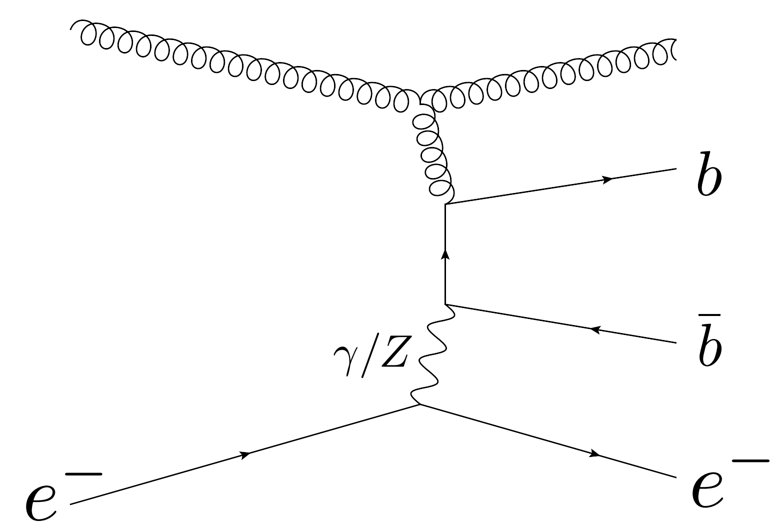

NC multi jets

https://indico.cern.ch/event/356714/contributions/844945/attachments/709283/973691/Updates_on_Hbb_studies.pdf

Masahiro Tanaka, Masahiro Kuze, Masaki Ishitsuka (Tokyo Institute of Technology)
Uta Klein (Liverpool University)
25 June 2015, LHeC Workshop 2015 @CERN and Chavannes-de-Bogis

- Mass reconstructed with 1st and 2nd minimum η b-jets.
- Signal region is defined as [100,130] GeV.

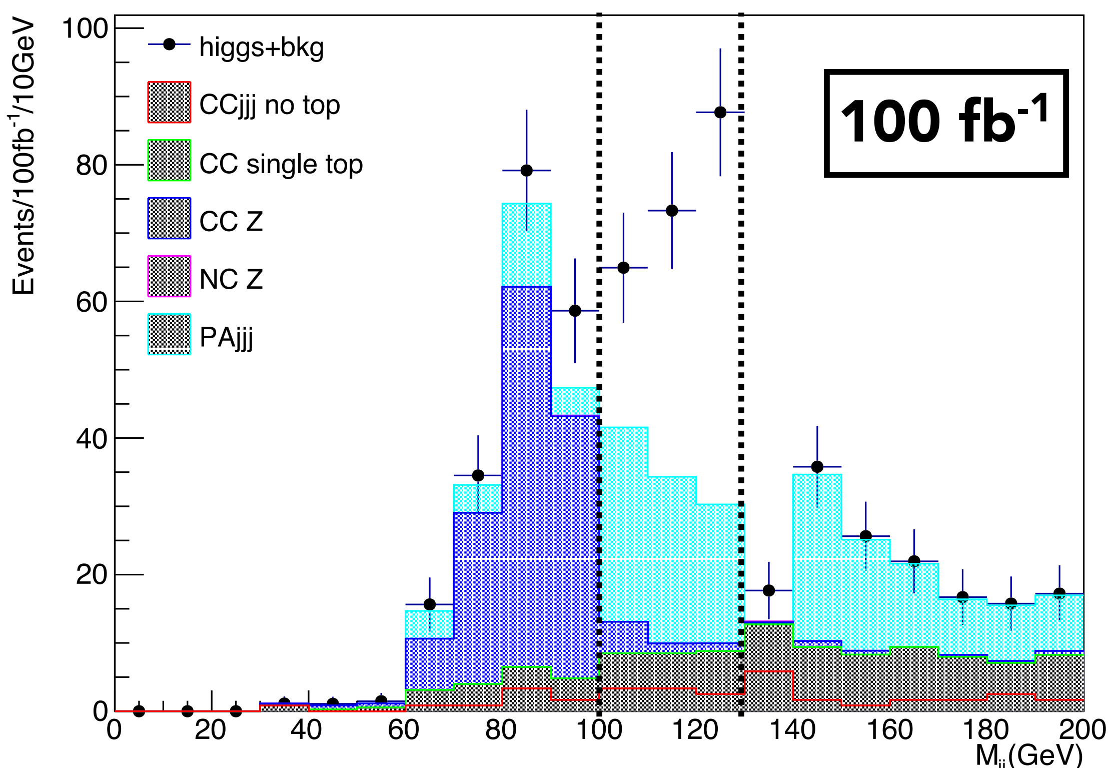

Events in signal region

Signal H->bb	119±2
CCjjj no top	9±3
CC single top	17±2
CC Z	7±1
NC Z	0
PAjjj	73±17
CCbkg total	33±4
NCbkg total	73±17

- Errors are weighted

S/√B = 11.5

- We can detect H->bb signal in good efficiency.
- Peak around 80 GeV is Z boson from CC background.
- PAjjj background has large statistical error due to small statistics.
- Electron tagging of Photo-production events could further suppress BG under peak.

Analysis Framework and *Detector**

Event generation

- **SM or BSM production**
- **CC & NC DIS background**

by MadGraph5/MadEvent

↓

- **Fragmentation**
- **Hadronization**

by PYTHIA **(modified for ep)***

↓

Fast detector simulation

by Delphes

→ test of LHeC detector

↓

S/B analysis → cuts or BDT

- Calculate cross section with tree-level Feynman diagrams (any UFO) using pT of scattered quark as scale (CDR $\hat{s}$) for ep processes with **MadGraph5** ; parton-level x-check CompHep
- Fragmentation & hadronisation uses **ep-customised** Pythia.
- **Delphes 'detector'**

→displaced vertices and signed impact parameter distributions → studied for LHeC and FCC-eh SM Higgs; and for extrapolations [PGS for CDR and until 2014]

- 'Standard' GPD LHC-style detectors used and further studied based on optimising Higgs measurements, i.e. vertex resolution a la ATLAS IBL, excellent hadronic and elmag resolutions using 'best' state-of-the art detector technologies (no R&D 'needed')
- Analysis requirements fed back to ep detector design

* See page 11 for ep Pythia checks
https://indico.cern.ch/event/278903/contributions/631181/attachments/510303/704309/Chavannes_UKLein_20.01.2014.pdf

Higgs in ep – clean S/B, no pile-up

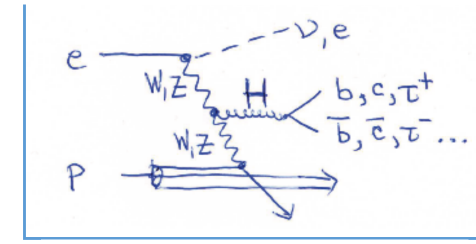

→ further improvements using BDT

realistic HFL tagging & BDT

Uta Klein & Daniel Hampson & Izzy Harris BSc 2017

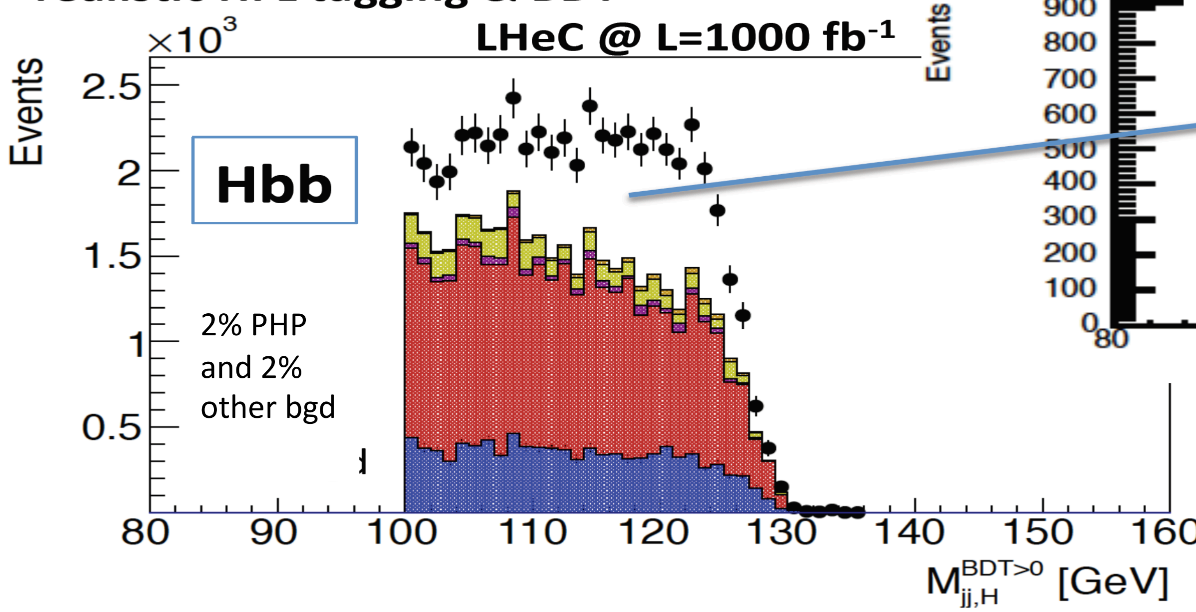

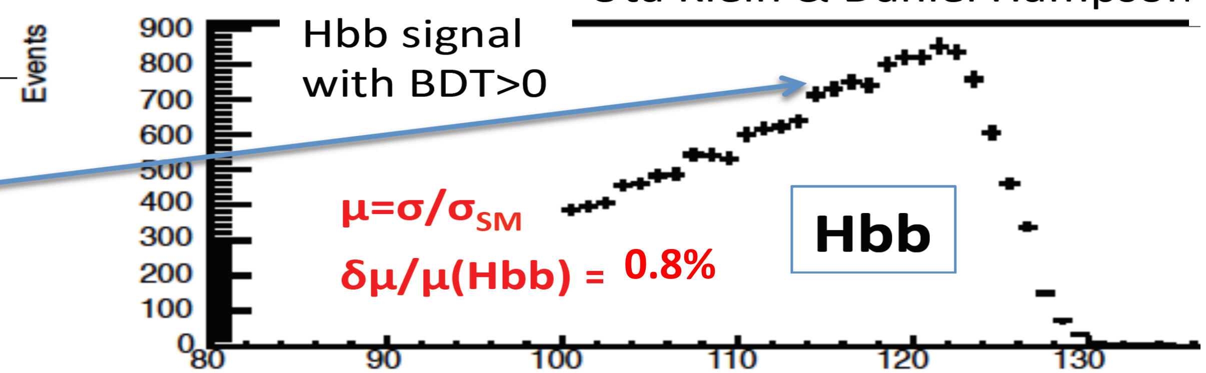

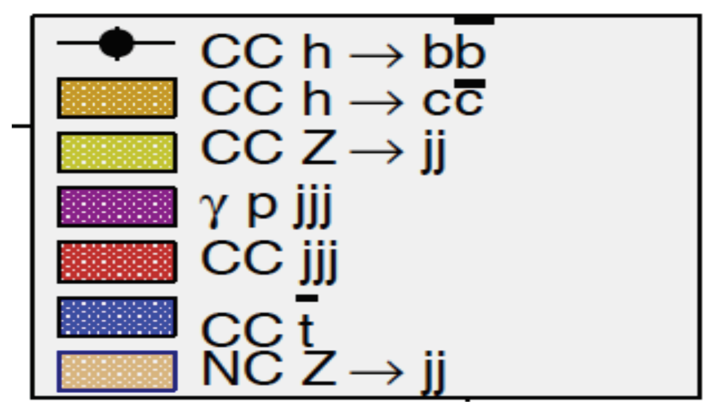

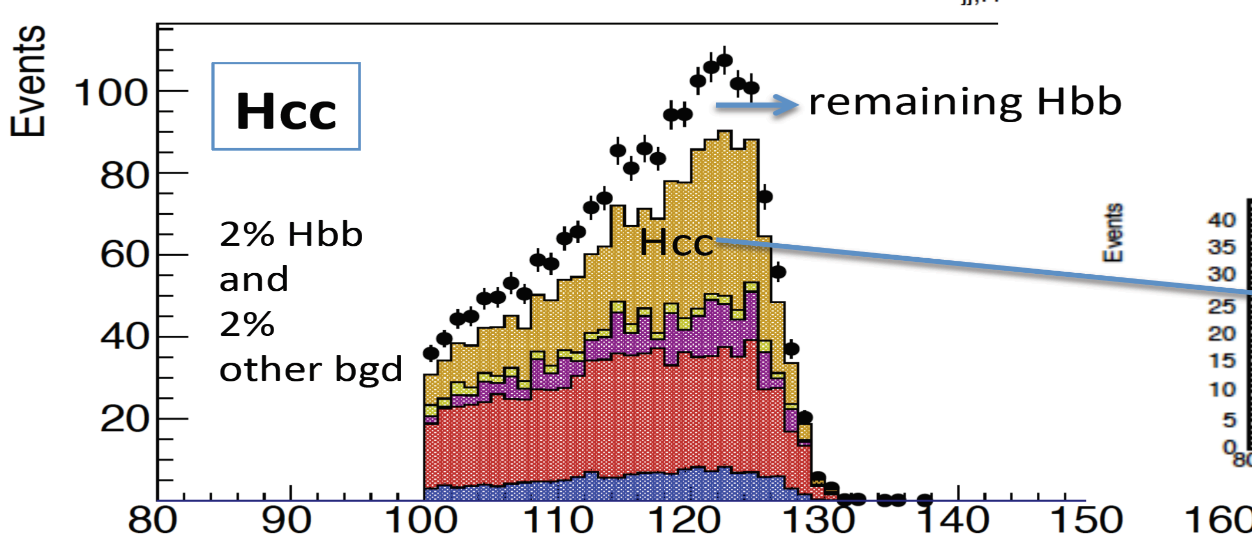

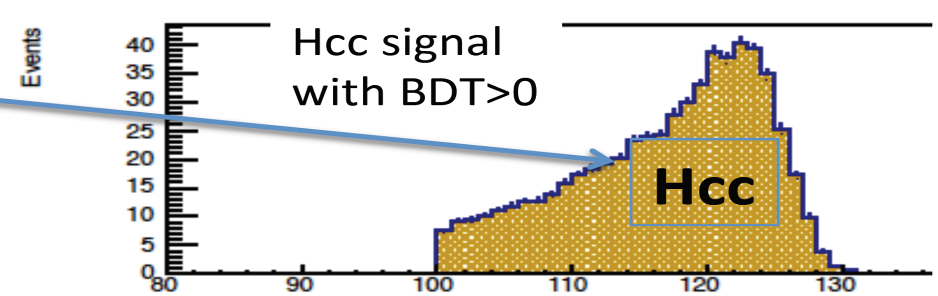

$\delta\mu/\mu(Hcc)$ = 7.4 %

Assuming background in control regions understood to 2% and negligible MC statistics for background in signal region; SM Higgs bb contribution in cc controlled by genuine Hbb measurement and b and c-jet correlation, see e.g. methodology ILC Hcc study arXiv: 0909.1052

[ILC Zqq-Hcc study got 8.8% for Hcc signal strength for M_H=120 GeV σ_{pol}(Hcc)=6.9 fb with similar Hcc, Hbb event numbers but factor 6.8 higher SM background than LHeC]

→ Main systematic checks: variations of background contribution and tagging efficiencies

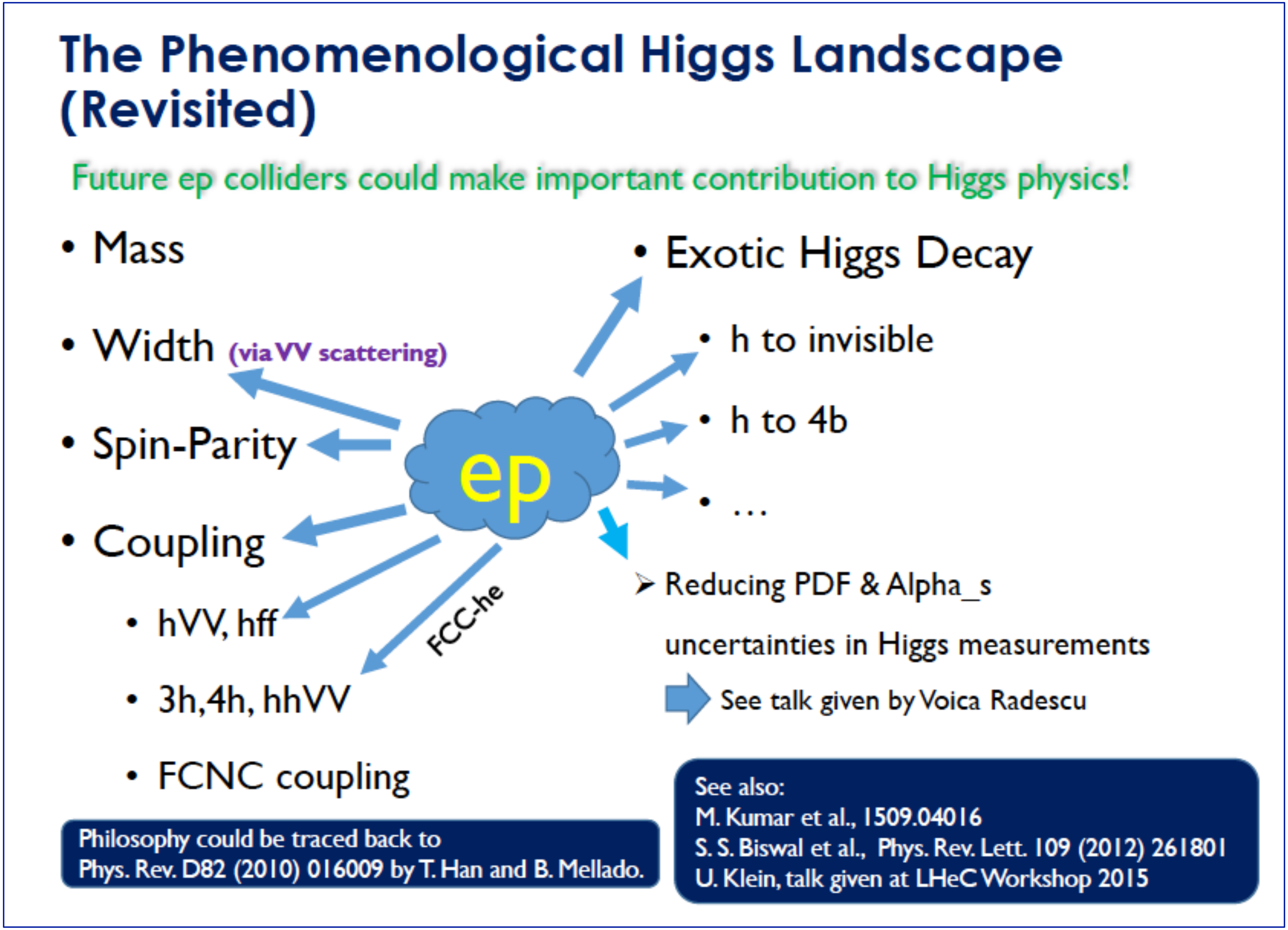

Chen Zhan 12.4.16 (talk at annual FCC week 2016, Rome)

Top Yukawa Coupling @ LHeC

B.Coleppa, M.Kumar, S.Kumar, B.Mellado, PLB770 (2017) 335

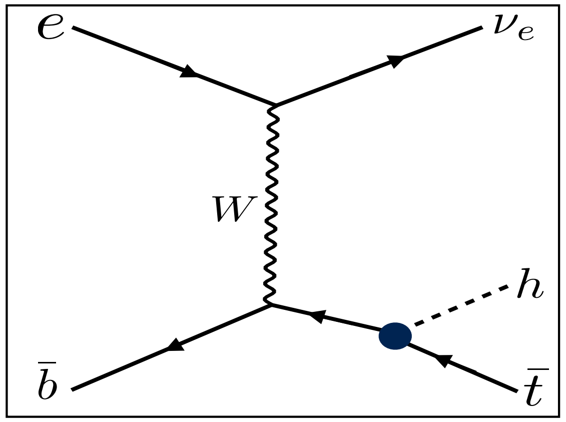

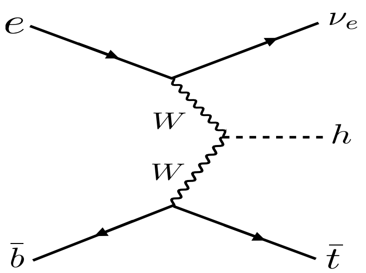

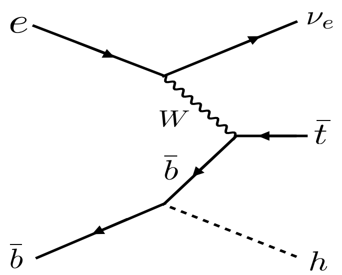

SM: $$\mathcal{L}_{\text{Yukawa}} = -\frac{m_t}{v}\bar{t}th - \frac{m_b}{v}\bar{b}bh,$$

BSM: Introduce phases of top-Higgs and bottom-Higgs couplings

$$\mathcal{L} = -\frac{m_t}{v}\bar{t}\,[\kappa\cos\zeta_t + i\gamma_5\sin\zeta_t]t\,h$$
$$-\frac{m_b}{v}\bar{b}\,[\cos\zeta_b + i\gamma_5\sin\zeta_b]b\,h.$$

Enhancement of the DIS cross-section as a function of phase

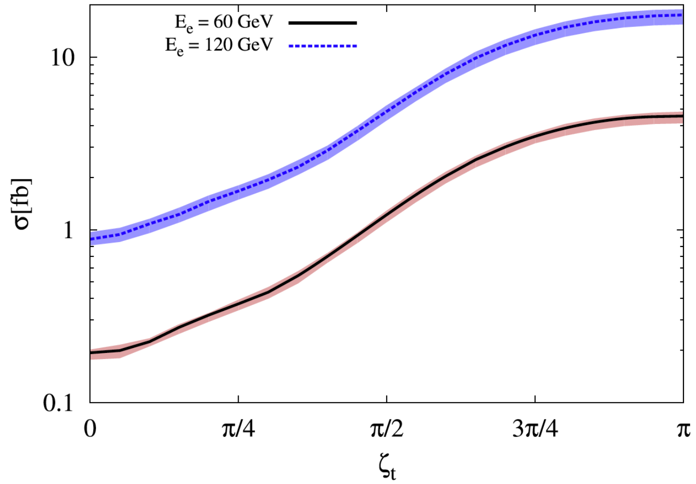

CP even sign flip $\zeta_{t,b} = \pi$

CP odd $\zeta_{t,b} = \frac{\pi}{2}$

CP even SM $\zeta_t = 0$

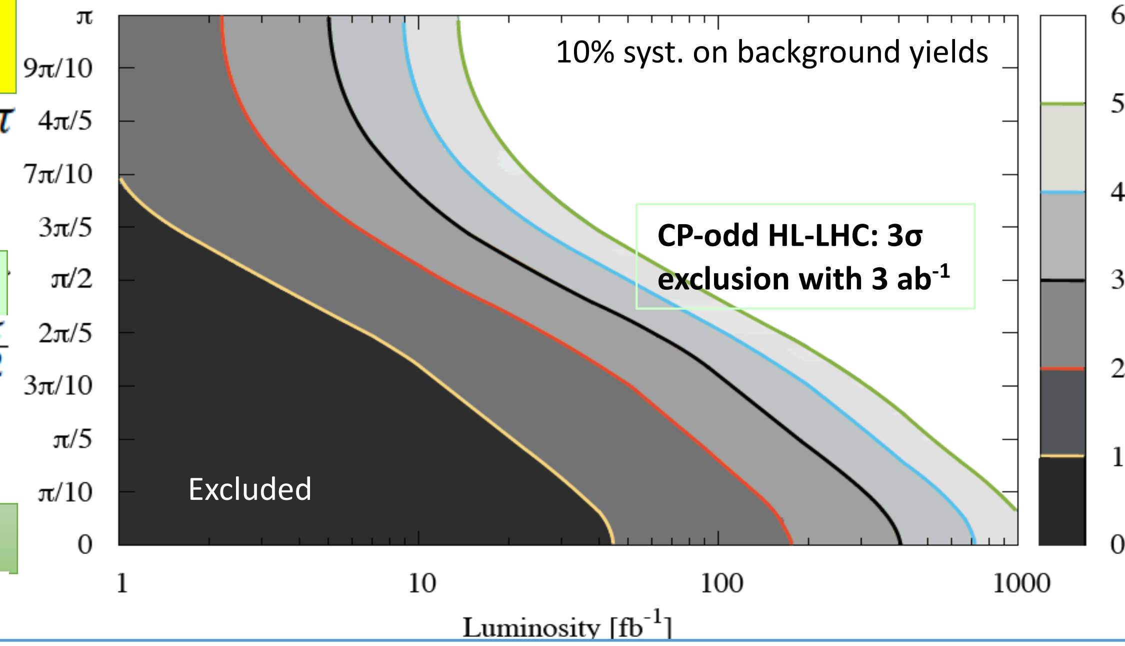

Observe/Exclude non-zero phase to better than 4σ
➔ With Zero Phase: Measure **ttH** coupling with **17% accuracy at LHeC** ➔ **extrapolation to FCC-eh: ttH to 1.7%**

Branching for invisible Higgs

Satoshi Kawaguchi,
Masahiro Kuze
Tokyo Tech

Values given in case of 2σ and L=1 ab^{-1}

Delphes detectors	LHeC [HE-LHeC] 1.3 [1.8 TeV]	FCC-eh 3.5 TeV
LHC-style	4.7% [3.2%]	1.9%
First 'ep-style'	5.7%	2.6%
+BDT Optimisation	5.5% (4.5%*)	1.7% (2.1%*)

LHeC parton-level, cut based <6% [Y.-L.Tang et al. arXiv: 1508.01095]

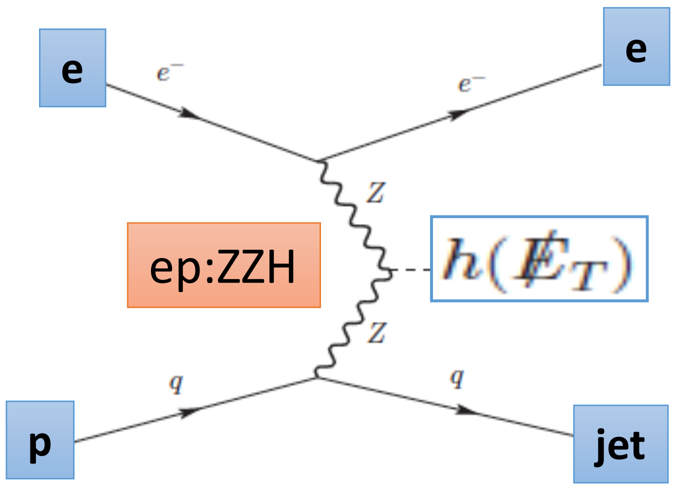

PORTAL to Dark Matter ?

- ✓ **Uses ZZH fusion process to estimate prospects of Higgs to invisible decay using *standard cut/BDT analysis techniques***
- ✓ **Full MG5+Delphes analyses, done for 3 c.m.s. energies → very encouraging for a measurement of the branching of Higgs to invisible in ep down to 5%** [1.2%] **for 1** [2] **ab^{-1} for LHeC** [FCC-eh]
- ✓ A lot of checks done: We also checked LHeC ←→ FCC-he scaling with the corresponding cross sections (* results in table) : Downscaling FCC-he simulation results to LHeC would give 4.5%, while up-scaling of LHeC simulation to FCC-he would result in 2.1% ➔ all well within uncertainties of projections of ~25%

➔ **further detector and analysis details have certainly an impact on results → enhance potential further**

BSM: channel h—> sb e. g. Cases in 2HDM-III

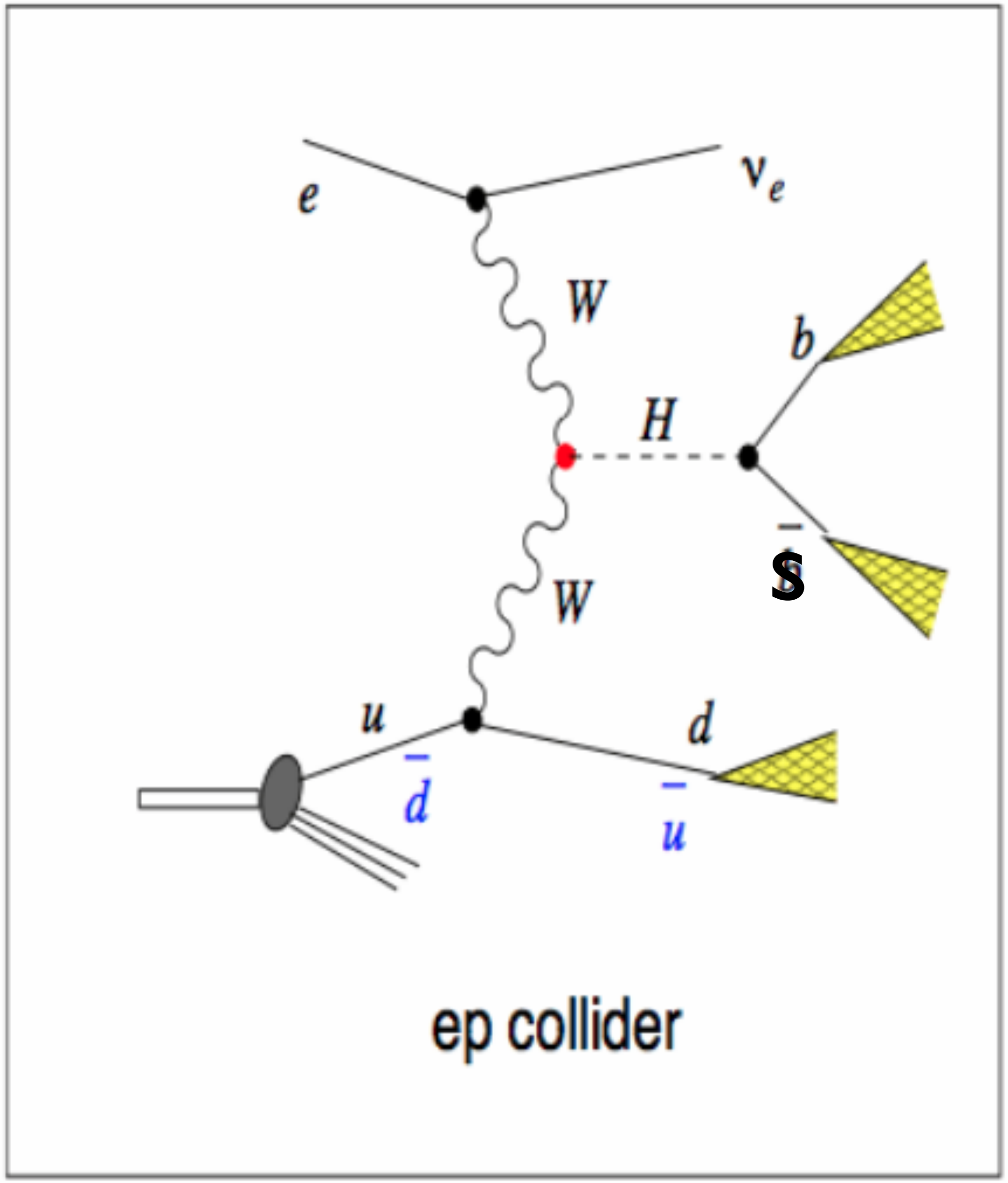

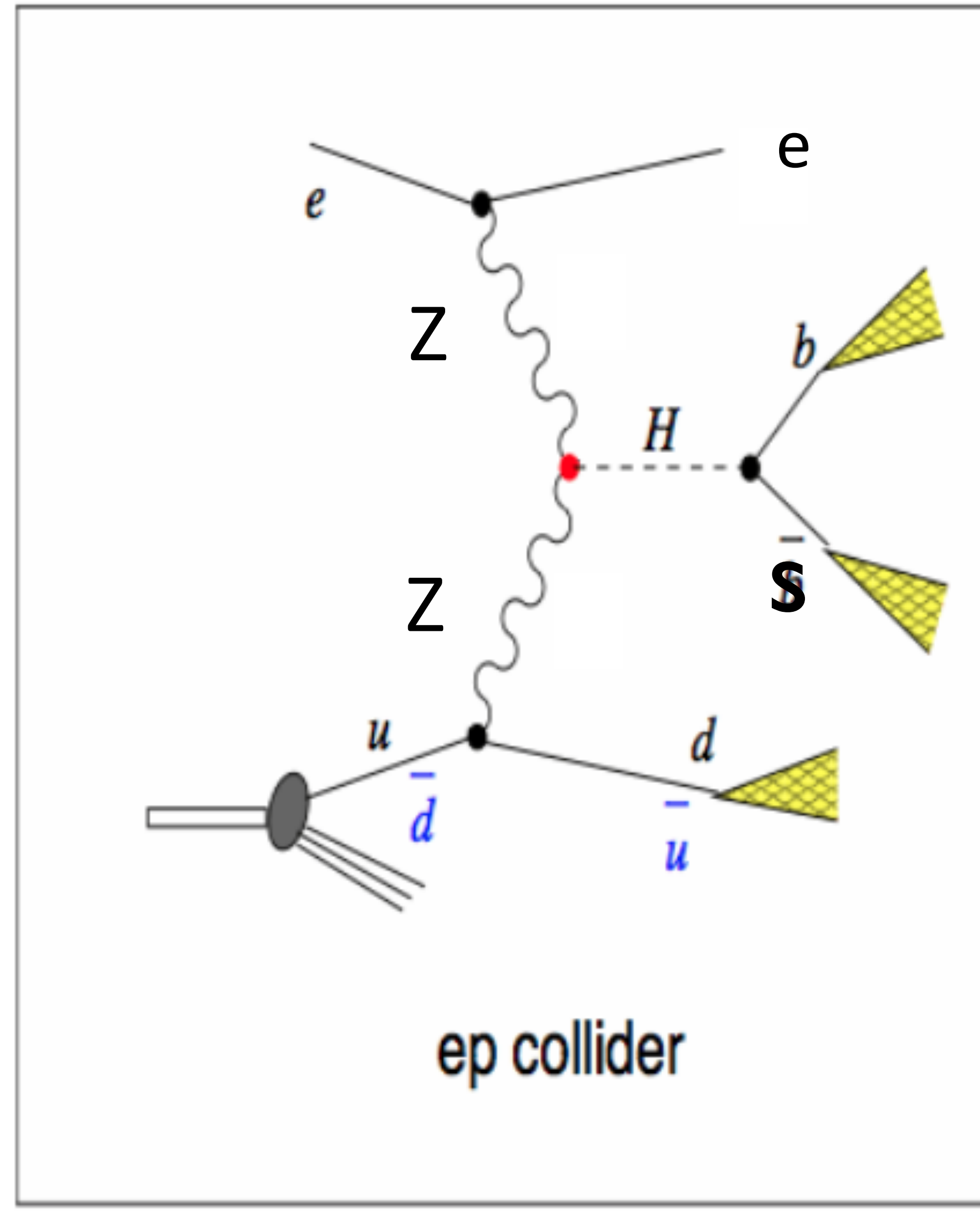

The background is reduced a lot

In the 2HDM; H= h0, H0

For H0 the coupling VVH0 is proportional to Cos(β-α) and VVh0 to Sin(β-α)

Further BSM Higgs Studies

Example: Charged Higgs

- $H\pm$, in Vector Boson Scattering

  [Georges Azuelos, Hao Sun, and Kechen Wang, 1712.07505]

- $H\pm\pm$, in Vector Boson Scattering

  [H. Sun, X. Luo, W. Wei and T. Liu, Phys. Rev. D 96, 095003 (2017)]

- H+, in 2HDM type III, $p\ e \rightarrow \nu j H \rightarrow \nu j\ cb$

  [J. Hernández-Sánchez et al., 1612.06316]

Production of H+ in ep collider

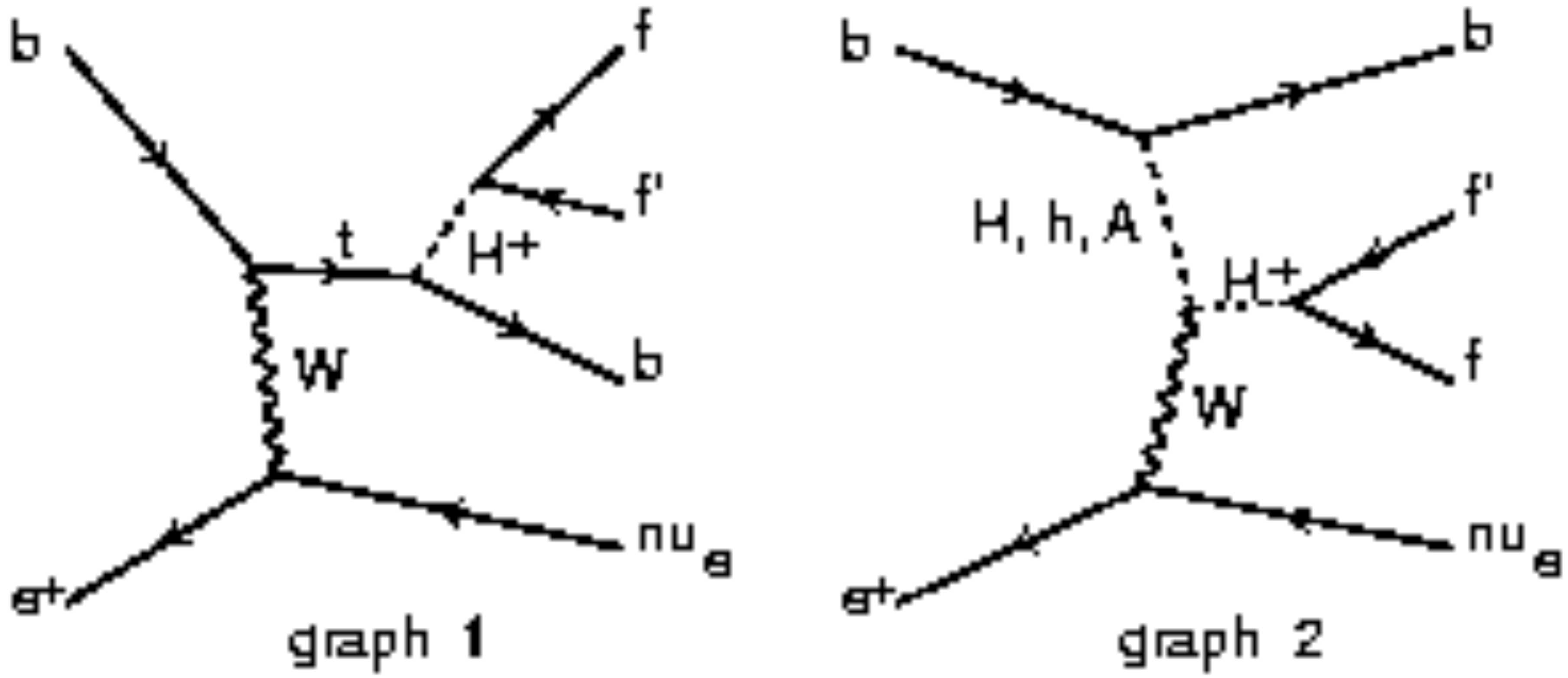

We focus in H+ —> cb, in 2HDM-III (also in MHDM) could be relevant

BR (H+ —> cb) ~ 0.9 in 2HDM-III
~0.8 in MHDM (A. Akeroyd, S. Moretti and J. Hernandez-Sanchez, PRD 85, 115002 (2012)) .

Higgs in ee vs ep

ee Dominant Higgs productions:

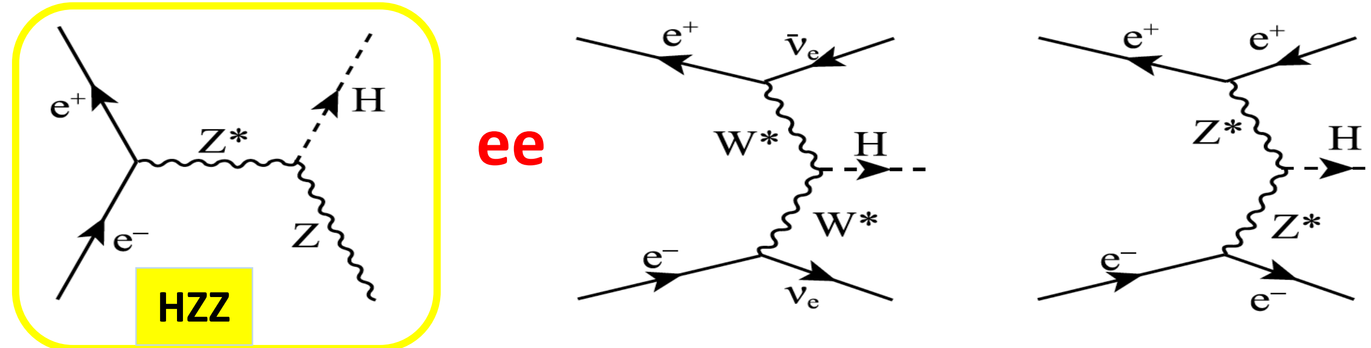

ep vs ee- Higgs cross sections

ep:CC DIS WW Fusion

ep: NC DIS ZZ Fusion

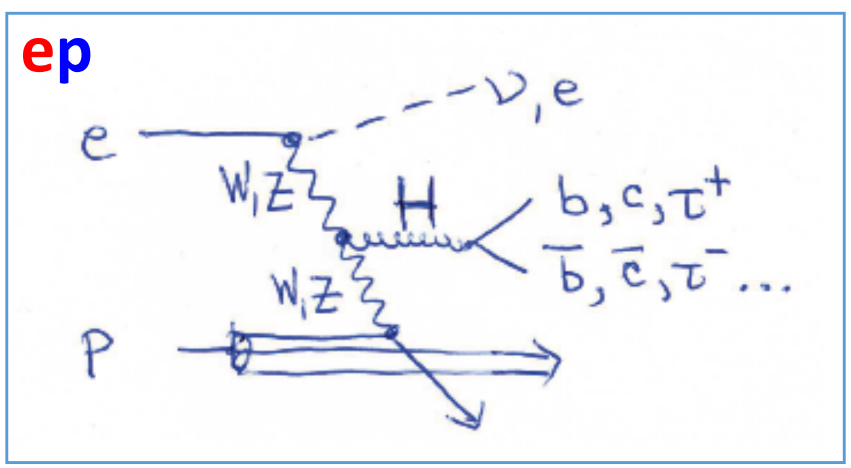

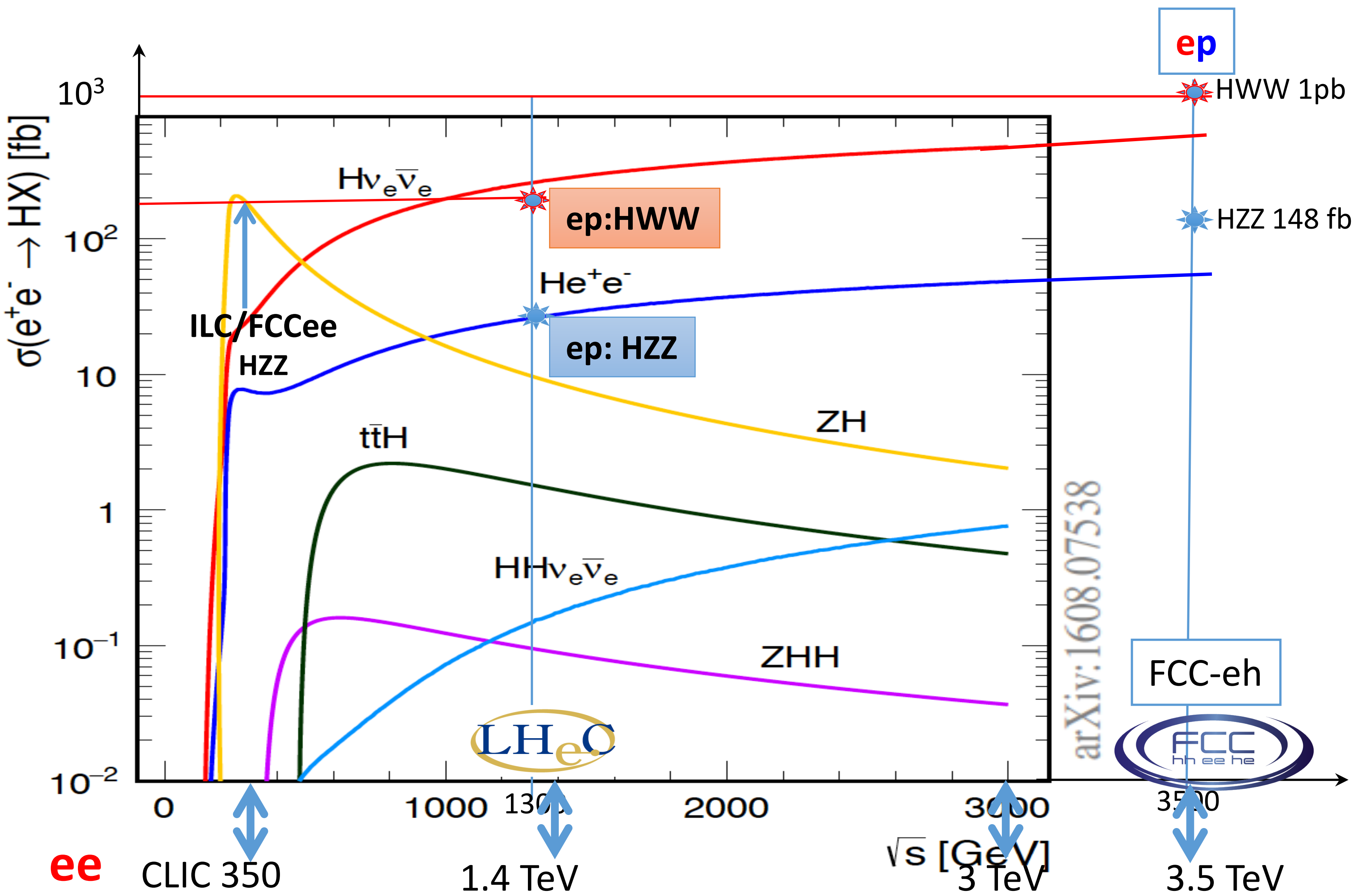

- **Current data (LEP/LHC) sensitive to NP in EW (Higgs) $\lesssim$1% (~10%)**

- **FCC can largely improve our knowledge of the EW/Higgs sectors. As with current data, no single machine can do all the work…**

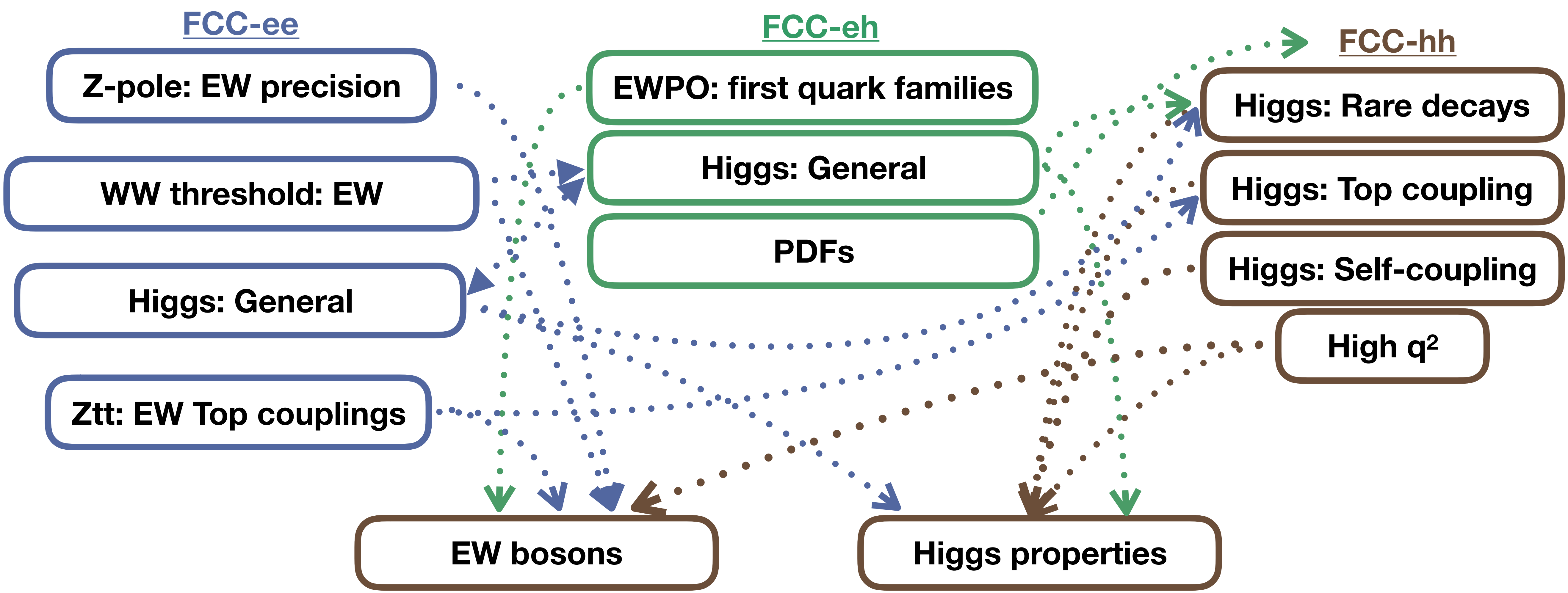

- **Apart from a strong EW/Higgs program, FCC-ee is also fundamental to maximize the physics output of the FCC-eh/hh**

Jorge de Blas (Talk at 11th FCCee workshop, CERN, 2019)

BSM: Some arguments o motivations 2HDM-III

The 2HDM-II could be transformed into 2HDM-III through the loops-effects of sfermions and gauginos

Andreas Crivellin, Phys.Rev. D83 (2011) 056001

In models with more than one Higgs doublet the MFV case is more stable in suppressing FCNCs than the hypothesis of NFC when the quantum corrections are taken into account.

A.J. Buras, M.V. Carlucci, S. Gori and G. Isidori, Higgs-mediated FCNCs: Natural Flavour Conservation vs. Minimal Flavour Violation , JHEP 10 (2010) 009 [arXiv:1005.5310].

Similar phenomenology in MHDM with flavor symmetries (Nearest-Neighbor-Interaction texture)

G. C. Branco, L. Lavoura and F. Mota, Phys. Rev. D 39, 3443 (1989)

Alfredo Aranda, Cesar Bonilla, J.Lorenzo Diaz-Cruz. Phys.Lett. B717 (2012) 248-251

2HDMs is studied in renormalization group evolution of the Yukawa couplings and the cases when the Z2-symmetry is broken, called non-diagonal models.

J. Bijnens, J. Lu and J. Rathsman, Constraining General Two Higgs Doublet Models by the Evolution of Yukawa Couplings , JHEP 05 (2012) 118

Yukawa textures in the 2HDM-III

The Yukawa textures are consistents with the relations between quarks masses and flavor mixing parameters.

Yukawa textures could come of a theory more fundamental and it could be a flavor symmetry.

H. Fritzsch, Z. Z. Xing, Prog.Part. Nucl. Phys. 45 (2000)1.
H. Fritzsch, Z. Z. Xing, Phys. Lett. 555 (2003)63.

Yukawa sector in 2HDM type III

$$\mathcal{L}_Y = Y_1^u \bar{Q}_L \Phi_1 u_R + Y_2^u \bar{Q}_L \Phi_2 u_R + Y_1^d \bar{Q}_L \Phi_1 d_R + Y_2^d \bar{Q}_L \Phi_2 d_R \, ,$$

$$(\tilde{Y}_2^l)_{ij} = \frac{\sqrt{m_i m_j}}{v} \tilde{\chi}_{ij} = \frac{\sqrt{m_i m_j}}{v} \chi_{ij} e^{\vartheta_{ij}},$$

The off-diagonal terms are constrained by CKM

$$M_f = \frac{1}{\sqrt{2}}(v_1 Y_1^f + v_2 Y_2^f), \qquad f = u, d, l,$$

$$\bar{M}_f = V_{fL}^\dagger M_f V_{fR}.$$

$$M_f = \begin{pmatrix} 0 & C_f & 0 \\ C_f^* & \tilde{B}_f & B_f \\ 0 & B_f^* & A_f \end{pmatrix}.$$

F. González, O. Félix-Beltrán, J.Hernandez-Sanchez, S. Moretti, R. Noriega, A. Rosado, Phys.Lett. B742 (2015) 347-352.
J. Hernandez-Sanchez, L. Lopez-Lozano, R. Noriega, A. Rosado, Phys.Rev. D85 (2012) 071301

Seesaw mechanism in MSSM

Flavor Violation among the Sleptons. In the leptonic sector, we begin with a Lagrangian:

$$-\mathcal{L} = \overline{E}_R Y_E L_L H_d + \overline{\nu}_R Y_\nu L_L + \frac{1}{2}\nu_R^\top M_R \nu_R \quad (1)$$

$$\frac{d}{d\log Q}(m_{\tilde{L}}^2)_{ij} = \left(\frac{d}{d\log Q}(m_{\tilde{L}}^2)_{ij}\right)_{\text{MSSM}} + \frac{1}{16\pi^2}\left[m_{\tilde{L}}^2 Y_\nu^\dagger Y_\nu + Y_\nu^\dagger Y_\nu m_{\tilde{L}}^2 + 2(Y_\nu^\dagger m_{\tilde{\nu}_R}^2 Y_\nu + m_{H_u}^2 Y_\nu^\dagger Y_\nu + A_\nu^\dagger A_\nu)\right]_{ij} \quad (2)$$

$$\left(\Delta m_{\tilde{L}}^2\right)_{ij} \simeq -\frac{\log(M/M_R)}{16\pi^2}\left(6m_0^2(Y_\nu^\dagger Y_\nu)_{ij} + 2\left(A_\nu^\dagger A_\nu\right)_{ij}\right) \quad (3)$$

where m_0 is a common scalar mass evaluated at the scale $Q = M$, and $i \neq j$. If we further assume that the A-terms are proportional to Yukawa matrices, then:

$$\left(\Delta m_{\tilde{L}}^2\right)_{ij} \simeq \xi \left(Y_\nu^\dagger Y_\nu\right)_{ij} \quad (4)$$

K.S. Babu, C. Kolda, Phys. Rev. Lett. 89,241802 (2002).

2HDM-III + Yukawa texture contain the following information:

It could come from a more fundamental theory (susy models with seesaw mechanism).

+

Yukawa texture is the flavor symmetry of the model and do not require of the discrete flavor symmetry.

+

The Higgs potential must be expressed in the most general form.

J. L. Diaz-Cruz, J. Hernandez-Sanchez, S. Moretti, R. Noriega, A. Rosado, Phys.Rev. D79 (2009) 095025
J. Hernandez-Sanchez, S. Moretti, R. Noriega-Papaqui, A. Rosado, JHEP 1307 (2013) 044

$$\mathcal{L}^{\bar{f}_i f_j \phi} = -\left\{ \frac{\sqrt{2}}{v} \overline{u}_i \left(m_{d_j} X_{ij} P_R + m_{u_i} Y_{ij} P_L \right) d_j \, H^+ + \frac{\sqrt{2} m_{l_j}}{v} Z_{ij} \overline{\nu_L} l_R H^+ + H.c. \right\}$$
$$-\frac{1}{v} \left\{ \bar{f}_i m_{f_i} h^f_{ij} f_j h^0 + \bar{f}_i m_{f_i} H^f_{ij} f_j H^0 - i \bar{f}_i m_{f_i} A^f_{ij} f_j \gamma_5 A^0 \right\},$$

where ϕ^f_{ij} ($\phi = h, H, A$), X_{ij}, Y_{ij} and Z_{ij} are defined as:

$$\phi^f_{ij} = \xi^f_\phi \delta_{ij} + G(\xi^f_\phi, X), \quad \phi = h, H, A,$$
$$X_{ij} = \sum_{l=1}^{3} (V_{\rm CKM})_{il} \left[X \frac{m_{d_l}}{m_{d_j}} \delta_{lj} - \frac{f(X)}{\sqrt{2}} \sqrt{\frac{m_{d_l}}{m_{d_j}}} \tilde{\chi}^d_{lj} \right],$$
$$Y_{ij} = \sum_{l=1}^{3} \left[Y \delta_{il} - \frac{f(Y)}{\sqrt{2}} \sqrt{\frac{m_{u_l}}{m_{u_i}}} \tilde{\chi}^u_{il} \right] (V_{\rm CKM})_{lj},$$
$$Z^l_{ij} = \left[Z \frac{m_{l_i}}{m_{l_j}} \delta_{ij} - \frac{f(Z)}{\sqrt{2}} \sqrt{\frac{m_{l_i}}{m_{l_j}}} \tilde{\chi}^l_{ij} \right].$$

With this structure in different limits one can have different 2HDM

$$\left(g^{f_u i f_d j H^+}_{2HDM-III} = g^{f_u i f_d j H^+}_{2HDM-any} + \Delta g^{f_u i f_d j H^+} \right)$$

J. Hernandez-Sanchez, S. Moretti, R. Noriega-Papaqui, A. Rosado, JHEP07 (2013) 044

2HDM-III	X	Y	Z	ξ_h^u	ξ_h^d	ξ_h^l	ξ_H^u	ξ_H^d	ξ_H^l
2HDM-I-like	$-\cot\beta$	$\cot\beta$	$-\cot\beta$	c_α/s_β	c_α/s_β	c_α/s_β	s_α/s_β	s_α/s_β	s_α/s_β
2HDM-II-like	$\tan\beta$	$\cot\beta$	$\tan\beta$	c_α/s_β	$-s_\alpha/c_\beta$	$-s_\alpha/c_\beta$	s_α/s_β	c_α/c_β	c_α/c_β
2HDM-X-like	$-\cot\beta$	$\cot\beta$	$\tan\beta$	c_α/s_β	c_α/s_β	$-s_\alpha/c_\beta$	s_α/s_β	s_α/s_β	c_α/c_β
2HDM-Y-like	$\tan\beta$	$\cot\beta$	$-\cot\beta$	c_α/s_β	$-s_\alpha/c_\beta$	c_α/s_β	s_α/s_β	c_α/c_β	s_α/s_β

- $\mu - e$ universality in τ decays
- Leptonic meson decays $B \to \tau\nu$, $D \to \mu\nu$, $D_s \to \mu\nu, \tau\nu$ and semileptonic decays $B \to D\tau\nu$
- $B \to X_s\gamma$ decays
- $B^0 - \bar{B}^0$ mixing
- Eelectro-weak precision test(including S,T,U oblique parameters)

Finally with all these above constraints one can find: $\chi^f_{kk} \sim 1$ and $|\chi^f_{ij}| \leq 0.5$,

The 2HDM-III as effective Lagrangian that induce at tree level flavor violating signatures like h,H —> sb, τμ and H+ —> cb, ts, decays can be relevant in the parameter space of the model.

$$\mathrm{BR}(B \to X_s\gamma)_{NLO} = B_{SL} \left|\frac{V_{ts}^* V_{tb}}{V_{cb}}\right|^2 \frac{6\alpha_{em}}{\pi\theta(z)\kappa(z)} \left[|D|^2 + A + \Delta\right],$$

$$\delta C^{0,eff}_{(7,8)}(\mu_W) = \left|\frac{Y^u_{33}Y^{u*}_{32}}{V_{tb}V_{ts}}\right| C^0_{(7,8),YY}(y_t) + \left|\frac{X^u_{33}Y^{u*}_{32}}{V_{tb}V_{ts}}\right| C^0_{(7,8),XY}(y_t),$$

$$\left|\frac{Y_{33}Y^*_{32}}{V_{tb}V_{ts}}\right| = \left[\left(Y - \frac{f(y)}{\sqrt{2}}\chi^u_{33}\right) - \sqrt{\frac{m_c}{m_t}}\left(\frac{V_{cb}}{V_{tb}}\right)\frac{f(Y)}{\sqrt{2}}\chi^u_{23}\right]\left[\left(Y - \frac{f(y)}{\sqrt{2}}\chi^u_{33}\right) - \sqrt{\frac{m_c}{m_t}}\left(\frac{V_{cs}}{V_{ts}}\right)\frac{f(Y)}{\sqrt{2}}\chi^u_{23}\right]^*,$$

$$\left|\frac{X_{33}Y^*_{32}}{V_{tb}V_{ts}}\right| = \left[\left(X - \frac{f(X)}{\sqrt{2}}\chi^d_{33}\right) - \sqrt{\frac{m_s}{m_b}}\left(\frac{V_{ts}}{V_{tb}}\right)\frac{f(X)}{\sqrt{2}}\chi^d_{23}\right]\left[\left(Y - \frac{f(y)}{\sqrt{2}}\chi^u_{33}\right) - \sqrt{\frac{m_c}{m_t}}\left(\frac{V_{cs}}{V_{ts}}\right)\frac{f(Y)}{\sqrt{2}}\chi^u_{23}\right]^*,$$

$B^0 - \bar{B}^0$ **mixing**

$$\left|\frac{Y_{33}Y^*_{32}}{V_{tb}V_{ts}}\right| < 0.25, \qquad -1.7 < Re\left[\frac{X_{33}Y^*_{32}}{V_{tb}V_{ts}}\right] < 0.7.$$

$(80 \text{ GeV} \leq m_{H^\pm} \leq 300 \text{ GeV})$.

As the four-zero texture controls the FCNC, then the most general Higgs potential could be considered for the 2HDM-III

$$
\begin{aligned}
V(\Phi_1,\Phi_2) = {} & \mu_1^2(\Phi_1^\dagger\Phi_1) + \mu_2^2(\Phi_2^\dagger\Phi_2) - \left(\mu_{12}^2(\Phi_1^\dagger\Phi_2) + \text{H.c.}\right) + \frac{1}{2}\lambda_1(\Phi_1^\dagger\Phi_1)^2 \\
& + \frac{1}{2}\lambda_2(\Phi_2^\dagger\Phi_2)^2 + \lambda_3(\Phi_1^\dagger\Phi_1)(\Phi_2^\dagger\Phi_2) + \lambda_4(\Phi_1^\dagger\Phi_2)(\Phi_2^\dagger\Phi_1) \\
& + \left(\frac{1}{2}\lambda_5(\Phi_1^\dagger\Phi_2)^2 + \left(\lambda_6(\Phi_1^\dagger\Phi_1) + \lambda_7(\Phi_2^\dagger\Phi_2)\right)(\Phi_1^\dagger\Phi_2) + \text{H.c.}\right)
\end{aligned}
$$

The custodial symmetry, pertubativity and unitarity are imposed and we obtain the following parameters of Higgs potential:

$$\text{for } \tan\beta \leq 10: \qquad |\lambda_{6,7}| \leq 1, \qquad \lambda_6 = -\lambda_7,$$

$$\sin(\beta-\alpha) \sim 1, \qquad \mu_{12} \sim v,$$

The masses of ma, mH+ and MH are chosen by STU obliques parameters

A. Cordero-Cid, J. Hernandez-Sanchez, C. Honorato, S. Moretti, A. Rosado, JHEP07 (2014) 057

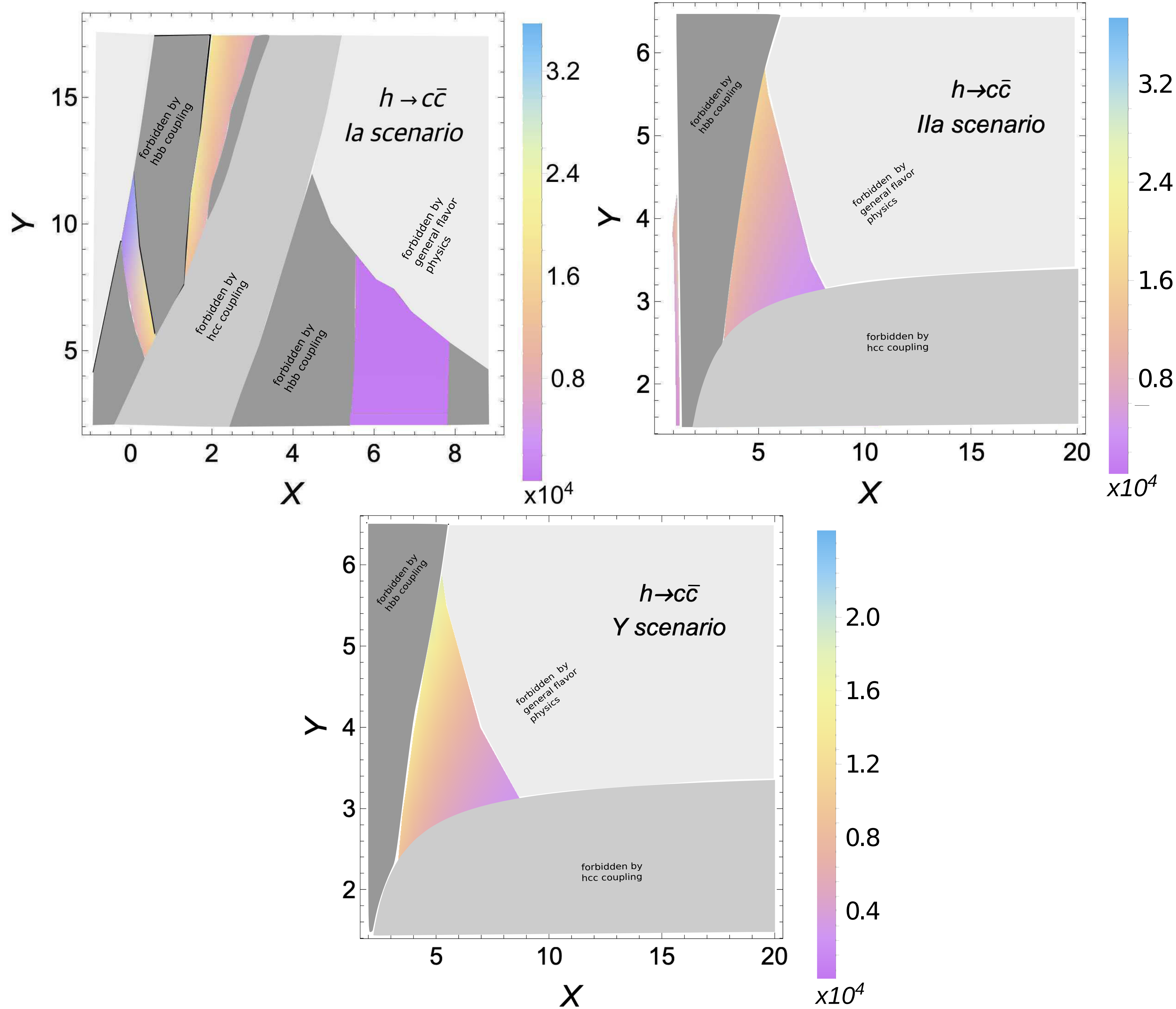

FIG. 1. Event rates for each benchmark scenario over the (X, Y) plane computed as $\sigma(ep \to \nu_e hj) \times \mathrm{BR}(h \to c\bar{c}) \times \epsilon_c^2 \times 1\ \mathrm{ab}^{-1}$. Here, we have $E_p = 50$ TeV and $E_{e^-} = 60$ GeV (with $P_L^{e^-} = -80\%$).

Limits for masses of neutral Higgs bosons:

An additional state with the same mass of the Higgs boson of SM is not ruled out, in particular the 2HDM-I could render it [arXiv:1307.1347 [hep-ph]].

CMS Collaboration analyse the range 110 GeV< M_H < 150 GeV in the almost case degenerate for the masses of Higgs boson, which is not excluded yet.

This result can be employed for CP-odd state.

Recently for CP-odd sate in any 2HDM, CMS has ruled out the range 225 GeV< m_A < 1000 GeV, considering low values of tan β [A. M. Sirunyan et al. (CMS), Eur. Phys. J. C 79, 564 (2019), arXiv:1903.00941 [hep-ex]].

Limits for masses of charged Higgs bosons:

CMS and ATLAS Collab-oration has imposed for the range of the mass 80 GeV < $m_{H^\pm}$ < 160 GeV, a higher limit for BR(t H+b) = 2 – 3%, assuming BR($H^+ \to \tau + \nu$) = 1 [V. Khachatryan et al. (CMS), JHEP 11, 018 (2015), arXiv:1508.07774 [hep-ex]],[M. Aaboud et al. (ATLAS), JHEP 09, 139 (2018), arXiv:1807.07915 [hep-ex]].

On the other hand, when BR($H^+ \to c\bar{s}$) = 1 is assumed, CMS collaboration establish BR($t \to H^+ b$)~20%in the mass range 90GeV<$m_{H^\pm}$<160 GeV [V.Khacha- tryan et al. (CMS), JHEP 12, 178 (2015), arXiv:1510.04252 [hep-ex]], [A. M. Sirunyan et al. (CMS), Phys. Rev. D 102, 072001 (2020), arXiv:2005.08900 [hep-ex]].

Besides, for the case BR($H^+ \to c\bar{b}$) = 1 and in the mass range 90GeV<$m_{H^\pm}$<160GeV, CMS give us a limit for BR(t H+b) ~ 0.5 – 0.8% [A. M. Sirunyan et al. (CMS), JHEP 11, 115 (2018), arXiv:1808.06575 [hep-ex]].

Lastly, very recently ATLAS collaboration has reported limits for the product of branching fractions BR(t H+b) × BR($H^+ \to c\bar{b}$) = 0.15% – 0.42% in the mass range 60 GeV < $m_{H^\pm}$ < 160 GeV, also reporting a slight excess in $m_{H^\pm}$ = 130 GeV [Collaboration (ATLAS), ATLAS-CONF-2021-037 (2021)].

Process: $e^- p \to \nu_e \phi q_f;\ \phi \to b\bar{s}$ +h.c.

These processes lead to 3-jets+ $\not{E}_T$

We demanded two jets in the central rapidity region: one tagged b-jet and one low flavor jet.

The remaining jet (q_f) has been tagged in the forwards region and the central jet veto (no more than one low flavor jet): are criterions to enhance the signal to the SM backgrounds.

TABLE I. Parameters for few optimistic benchmark points in the 2HDM-III as a 2HDM-I, -II and -Y configuration. Here bs stands for $\mathrm{BR}(\phi \to b\bar{s} + \bar{b}s)$, in units of 10^{-2}, where $\phi = h, H$, while $\sigma.bs$ stands for the cross section multiplied by the above BR as obtained at the LHeC in units of fb. We have analyzed only the benchmarks where the $\sigma.bs$ is greater than 0.15 fb, so that at least 15 events are produced for 100 fb^{-1}.

				$m_h = 125$ GeV		$m_H = 130$ GeV		$m_H = 150$ GeV		$m_H = 170$ GeV	
2HDM	X	Y	Z	bs	$\sigma.bs$	bs	$\sigma.bs$	bs	$\sigma.bs$	bs	$\sigma.bs$
Ib35	28	10	28	15.66	6.392	51.8	1.209	51.6	0.30	1.58	0.117
Ib47	30	5	30	16.14	3.086	48.2	10.983	48.0	0.127	1.80	0.839
Ib57	44	5	44	17.58	11.861	38.6	5.14	38.4	2.303	3.68	0.137
IIa11	20	2	20	1.42	1.055	25.2	0.097	25.0	0.091	24.8	0.085
IIa14	26	2	26	1.44	1.651	26.0	0.059	25.8	0.054	25.6	0.049
IIa26	36	1	36	1.46	1.621	26.4	0.045	26.2	0.042	26.0	0.038
Ya11	20	2	−2	1.42	1.084	25.2	0.062	25.0	0.059	24.8	0.054
Ya12	22	2	−2	1.44	1.078	25.6	0.057	25.4	0.053	25.2	0.048
Ya14	26	2	−2	1.46	1.441	26.0	0.057	25.8	0.053	25.6	0.049

We consider only σ.bs > 0.15 fb; at least 15 events for 100 fb^(-1)

We applied the following basic preselections:

$$p_T^q > 15.0 \quad \mathrm{GeV}, \Delta R(q,q) > 0.4$$

$\Delta R = \Delta\eta^2 + \Delta\phi^2$, where η and ϕ are the pseudo-rapidity and azimuthal angle respectively.

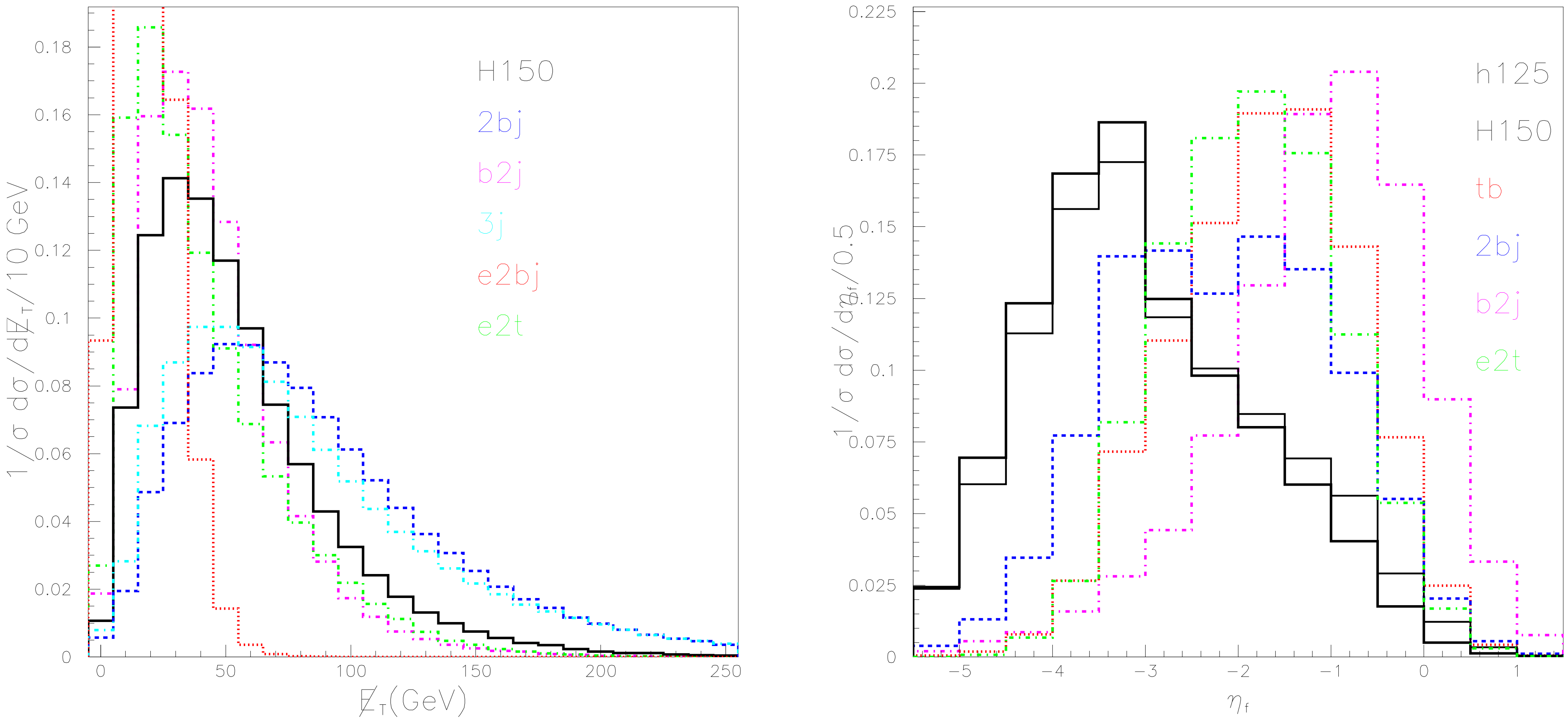

FIG. 9. The missing energy ($\not{E}_T$) (left panel) and rapidity (η_{j_f}) (right panel) profile of the forward jet for signals and SM backgrounds. The $\not{E}_T$ distributions for all other signal benchmarks as well as the $t\bar{b}$ noise are not shown as they are very similar to the signal distributions of m_H=150 GeV for Scenario Ib with $X = Z = 28$ and $Y = 10$ (shown in thick solid), whereas the thin solid is for m_h=125 GeV for Scenario Ia with $X = Z = 28$ with $Y = 10$. The rapidity distributions profile for m_H=130(170) GeV is very close to the m_h=125 GeV(m_H=130 GeV) case shown in thin solid, except that for massive Higgs the peaks shift towards the left. Also the corresponding rapidity distribution profile for *e2bj* is somewhat similar to the m_h=125 GeV signal case.

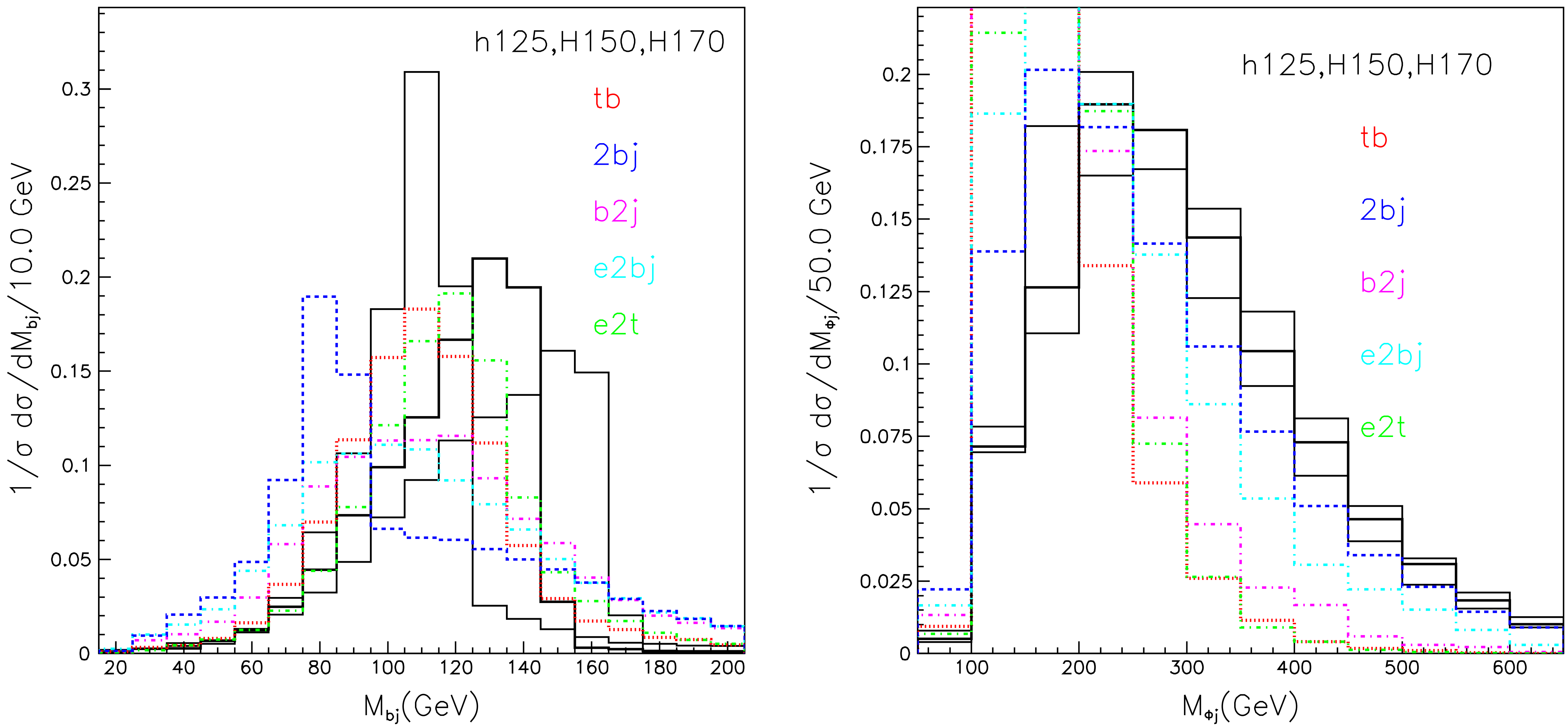

FIG. 6. The dijet invariant mass, made up by one b-tagged and one light-flavor jet, producing Higgs candidates, $M_\phi = M_{bj}$ (left panel) and the three-jet invariant mass, i.e., the previous two jets combined together with the forward jet, $M_{\phi j_f}$ (right panel). The mass peaks of the Higgs signals (M_ϕ) correspond to $m_h = 125$ (thin black) for Scenario Ia, $m_H = 150$ (thick black) and 170 (thin black) for Scenario Ib from left to right. All these are using the parameters $X = Z = 28$ and $Y = 10$. The distribution for $m_H = 130$ is not shown but it lies in between $m_h = 125$ and $m_H = 150$. Among all SM backgrounds, only $2bj$ shows a prominent peak from the Z-boson. Notice that $M_{\phi j_f}$ represents the overall energy scale of the hard-scattering.

h_{SM}=125 GeV:3-jet+$\not{E}_T$ with 100 fb^{-1}

Details in arXiv: 1503.01464
PRD 94, 055003 (2016)

- a: $N_j \gtrsim 3$
- b: $N_{b-tag} \gtrsim$ 1 (with ϵ_b=0.50, ϵ_c=0.10 and ϵ_j=0.01, where j=u,d,s,g)
- cd : at least two central jets (within $\eta < 2.5$) with $\not{E}_T > 20 GeV$ →3j not survive and photo production is reduced
- e: lepton (e or μ) veto with $p_T > 20$ GeV and $\eta < 3.0$
- f: in the central region: $|M_{bj} - M_{h(H)}|$ is minimum and with 15 GeV mass windows.
- g: remaining leading jet with $p_T > 25$ GeV and $-5.5 < \eta < -0.5$
- h: $m_{\phi j_f} > 190$ GeV

i: We required only one low flavored jet in the central regions (this has severe impact on the processes)

- S.P. Das, J. Hernández-Sánchez, S. Moretti, A. Rosado, R. Xoxocotzi

TABLE II. Expected number of events after different combinations of cuts for signal and backgrounds at the LHeC with an integrated luminosity of 100 fb^{-1} for $m_h = 125$ GeV. SimEvt stands for the actual number of events analyzed in the Monte Carlo simulations. RawEvt stands for the number of events with only the generator–level cuts (14) imposed; for the signal as well as for background, these are calculated from the total cross section times branching ratio. In the final column we mention the significances($\mathcal{S}$) defined as $\mathcal{S} = S/\sqrt{B}$, where S stands for signal events, background events B for 100 fb^{-1} of data after all cuts mentioned in the "i" column. The number in the parenthesis in the final column represent the significances for 1000 fb^{-1}.

Proc	SimEvt	RawEvt	a	b	c	d	e	f	g	h	i	$\mathcal{S}$
Ib35	100 K	639.2	447.6	177.3	117.1	97.4	93.8	37.8	31.7	25.4	15.8	1.2(3.8)
Ib47	100 K	308.6	216.8	85.1	56.2	47.1	45.5	18.4	15.6	13.0	8.1	0.62(2.0)
Ib57	100 K	1186.1	833.7	325.7	215.5	180.6	173.9	70.3	59.1	49.3	31.1	2.4(7.5)
IIa11	100 K	105.5	74.3	29.1	19.2	16.0	15.4	6.3	5.3	4.4	2.8	0.21(0.70)
IIa14	100 K	165.1	116.1	45.2	30.0	25.4	24.4	9.7	8.3	6.9	4.4	0.33(1.05)
IIa26	100 K	162.1	114.4	44.7	29.5	24.5	23.6	9.5	8.1	6.8	4.3	0.33(1.03)
Ya11	100 K	108.4	76.3	29.8	19.6	16.4	15.8	6.4	5.4	4.6	2.9	0.22(0.70)
Ya12	100 K	107.8	76.2	29.6	19.5	16.3	15.7	6.3	5.4	4.5	2.8	0.21(0.67)
Ya14	100 K	144.1	101.7	39.8	26.0	21.7	20.8	8.2	7.0	5.9	3.8	0.29(0.92)
$\nu t\bar{b}$	100 K	50712.1	28338.4	15293.7	9845.0	8144.2	7532.7	2982.1	2058.0	652.2	139.6	
$\nu b\bar{b}j$	560 K	14104.6	6122.8	3656.7	1858.5	1787.1	1650.1	257.5	152.5	85.2	15.1	
$\nu b2j$	90 K	18043.1	8389.2	3013.0	1691.5	1445.5	1373.7	389.5	206.1	77.2	11.3	$B = 170.8$
$\nu 3j$	300 K	948064.2	410393.4	15560.9	0.0	0.0	0.0	0.0	0.0	0.0	0.0	$\sqrt{B} = 13.1$
$eb\bar{b}j$	115 K	256730.1	55099.8	36353.6	12659.8	1432.0	200.7	54.1	24.8	18.0	4.5	
$et\bar{t}$	130 K	783.3	685.0	384.5	265.9	179.3	26.2	11.6	10.5	3.9	0.3	

TABLE III. Same as Table II but for $m_H = 130$ GeV. The criterion for jets and b-tagging are the same, so that the number of events in column A and B are the same for all SM backgrounds.

Proc	SimEvt	RawEvt	A	B	C	D	E	F	G	H	I	$\mathcal{S}$
Ib35	100 K	120.9	87.1	34.1	26.9	22.5	21.6	7.5	6.1	5.3	3.4	0.28(0.88)
Ib47	100 K	1098.3	790.3	307.1	243.9	204.6	195.7	68.5	56.1	48.6	31.3	2.6(8.1)
Ib57	100 K	514.0	371.2	144.8	115.0	96.0	92.0	31.7	25.8	22.7	14.3	1.2(3.7)
IIa11	100 K	9.7	6.8	2.7	2.1	1.8	1.7	0.6	0.4	0.3	0.2	0.02(0.05)
IIa14	100 K	5.9	4.2	1.7	1.3	1.1	1.0	0.4	0.3	0.2	0.1	0.01(0.02)
IIa26	100 K	4.5	3.1	1.3	1.0	0.8	0.8	0.3	0.2	0.1	0.1	0.01(0.02)
Ya11	100 K	6.2	4.4	1.8	1.4	1.1	1.1	0.4	0.3	0.2	0.1	0.01(0.02)
Ya12	100 K	5.7	4.0	1.6	1.3	1.0	1.0	0.3	0.2	0.2	0.1	0.01(0.02)
Ya14	100 K	5.7	4.0	1.6	1.3	1.0	1.0	0.3	0.2	0.2	0.1	0.01(0.02)
$\nu t\bar{b}$	100 K	50712.1	28338.4	15293.7	10976.4	9092.4	8393.6	2550.9	1565.5	617.9	113.7	
$\nu b\bar{b}j$	560 K	14104.6	6122.8	3656.7	2145.5	2062.1	1902.9	266.6	141.0	87.5	14.4	
$\nu b2j$	90 K	18043.1	8389.2	3013.0	2053.6	1734.0	1650.1	402.8	143.7	64.5	8.1	$B = 147.8$
$\nu 3j$	300 K	948064.2	410393.4	15560.9	0.0	0.0	0.0	0.0	0.0	0.0	0.0	$\sqrt{B} = 12.2$
$eb\bar{b}j$	115 K	256730.1	55099.8	36353.6	16838.4	1826.6	284.1	56.4	31.6	22.6	11.3	
$et\bar{t}$	130 K	783.3	685.0	384.5	280.8	190.8	27.8	10.9	9.3	3.9	0.3	

FCC-eh Collider

a) We require $N(j) = 3$ for the number of jets, one of which has to be b-tagged, and place a lepton veto $N(l) = 0$.
b) We select a missing energy $\not{E} > 20$ GeV and a hadronic tranverse energy $H_T > 130$ GeV.
c) We enforce the transverse momentum for the jets to be $p_T(j_b) > 30$ GeV , $p_T(j_1) > 40$ GeV and $p_T(j_2) > 30$ GeV.
d) We restrict the jet pseudo-rapidities as $|\eta(j_b)| < 2.5$, $|\eta(j_1)| < 2.5$ (central) and $|\eta(j_2)| > 1.5$ (forward).
e) We enable a cone separation amongst jets candidates to h o H $\Delta R(j_b, j_1) < 3$, it is a central di-jet. We enforce a isolation coditions for j_1 and j_2 $\Delta R(j_1, j_2) > 2.5$.
f) Finally, we sample on the di-jet invariant mass $(m_\phi - 25 \text{ GeV}) < M_{j_b j_1} < m_\phi$.

In this analysis we use Madgraph, with Pythia-PGS package.
We consider -80% longitudinally polarized electron beam.

2HDM-III	X	Y	Z	$m_h = 125$ GeV		$m_H = 130$ GeV		$m_H = 150$ GeV		$m_H = 170$ GeV	
				bs	$\sigma.bs$	bs	$\sigma.bs$	bs	$\sigma.bs$	bs	$\sigma.bs$
Ib57	44	5	44	93.22	784	20.2	46.06	17.12	33.56	3.54	6.05
IIa14	26	2	26	1.52	15.2	28.3	10.64	28.4	7.51	28.4	5.72

TABLE I. FCC-eh rates for our 2HDM-III BPs, where bs stands for BR($\phi \to b\bar{s} + \bar{b}s$) in units of 10^{-2} while σ.bs stands for the cross section $\sigma(ep \to \nu_e \phi q)$ (q = light flavor quark) times the above BR in units of fb.

FCC-eh Collider

S	Higgs mass	RawEvt	a	b	c	d	e	f	Σ
Ib57	$m_h = 125$ GeV	784 k	21598	11841	6487	2875	1618	1038	11.17(19.36)
	$m_H = 130$ GeV	228k	3732	2217	1237	548	299	221	2.38(4.12)
	$m_H = 150$ GeV	196k	2935	1789	1024	511	265	93	1.75(3.02)
	$m_H = 170$ GeV	171k	1026	538	260	146	69	15	0.29(0.51)
IIa14	$m_h = 125$ GeV	1000 k	56973	31397	17146	7346	3905	2600	28(48.5)
	$m_H = 130$ GeV	37.6k	2078	1236	698	353	130	67	0.72(1.25)
	$m_H = 150$ GeV	26.4k	1364	941	573	312	129	30	0.56(0.98)
	$m_H = 170$ GeV	20.17k	1043	778	499	285	124	25	0.49(0.85)
$\nu t\bar{b}$		13050k	415871	217059	107189	53849	16461	3956	
$\nu b\bar{b}j$		370k	19966	11621	5695	2231	814	488	
$\nu b2j$		170k	3737	1348	603	284	114	23	$B = 8622$
$\nu 3j$		92100k	837783	310678	111704	48871	23563	3927	$\sqrt{B} = 92.85$
$eb\bar{b}j$		44800k	222537	17329	6384	3420	1596	228	
$et\bar{t}$		395k	134	95	67	36	12	0	

FCC-eh with $L = 1(3)$ ab^{-1}.

Submitted to CDR of FCC-eh

FCC-eh Collider

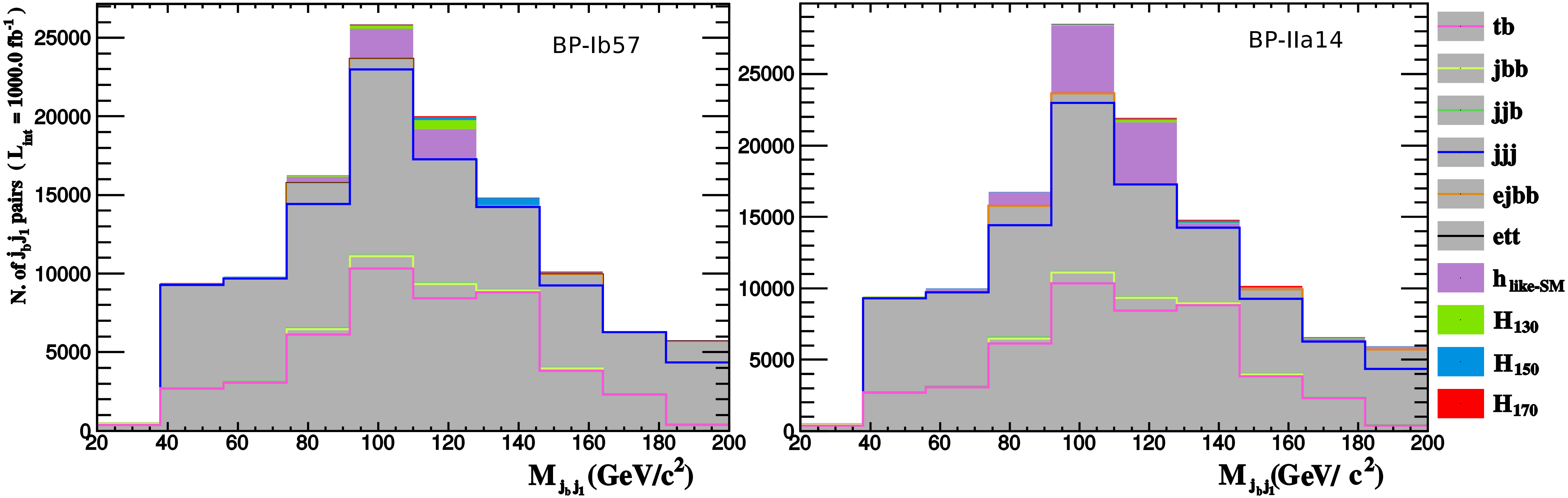

The $M_{j_b j_1}$ distribution for S and B after all cuts in Tab. II with $L = 3$ ab^{-1} for both BP

Production of H- in ep collider

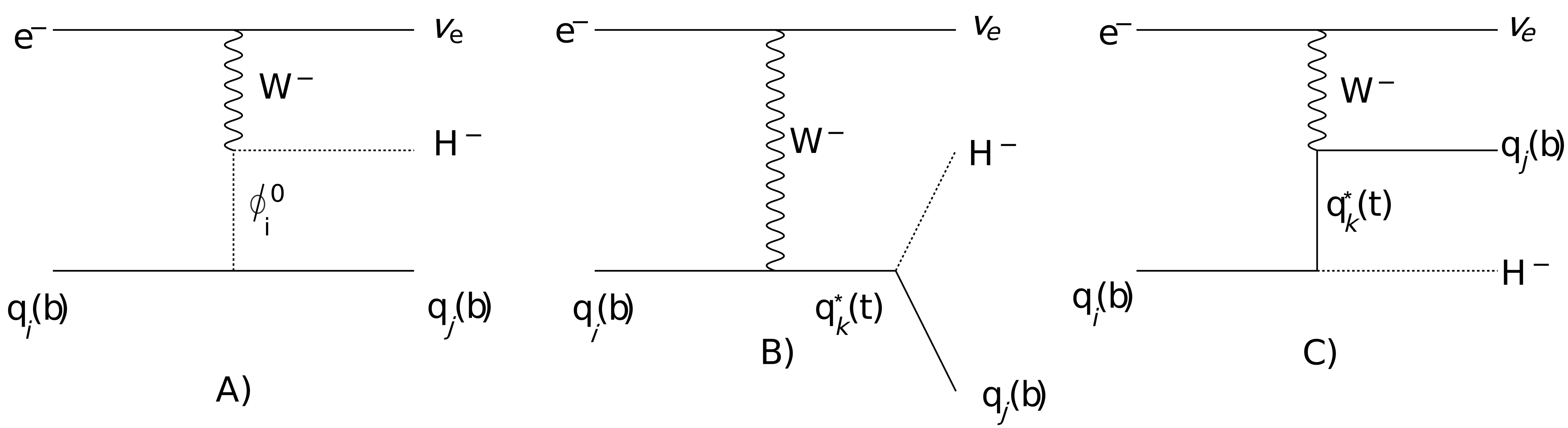

FIG. 1. Feynman diagrams for the $e^- \; p \to \nu_e H^- q$ process. Here, $\phi_i^0 = h, H, A$, i.e., any of the neutral Higgs bosons of the BSM scenario considered here (see below).

J. Hernandez-Sanchez, C.G. Honorato, S. Rosado, S. Moretti,
Phys.Rev.D 99 (2019) 9, 095009

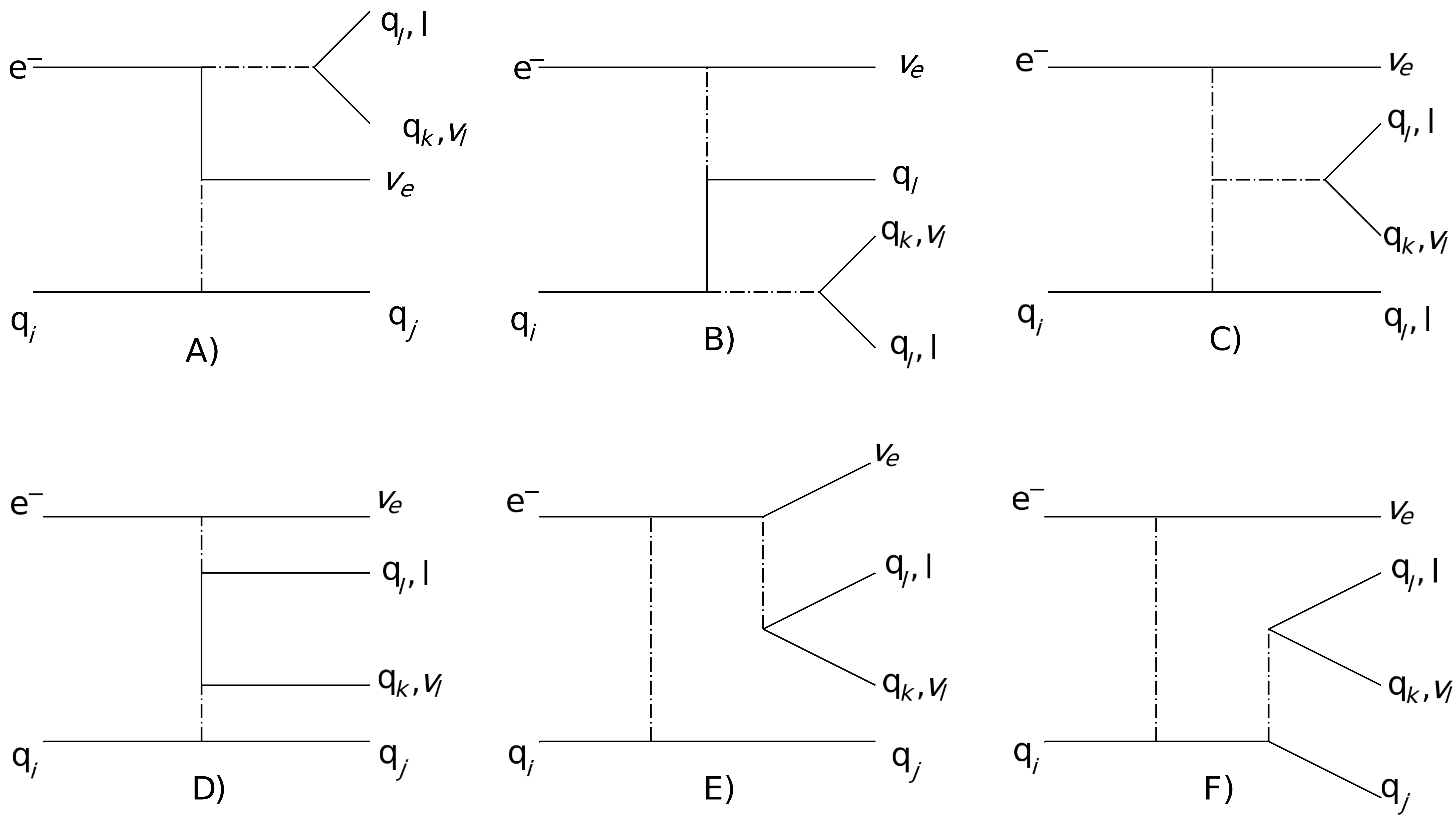

FIG. 2. Feynman diagrams for the $\nu_e jjj$, $\nu_e bjj$ and $\nu_e bbj$ backgrounds (the change $q_l \leftrightarrow l$ and $q_k \leftrightarrow \nu_l$ represents the $\nu_e \nu_l lj$ and $\nu_e \nu_l lb$ backgrounds). Dash-dot lines represent boson fields: (pseudo)scalars and EW gauge bosons.

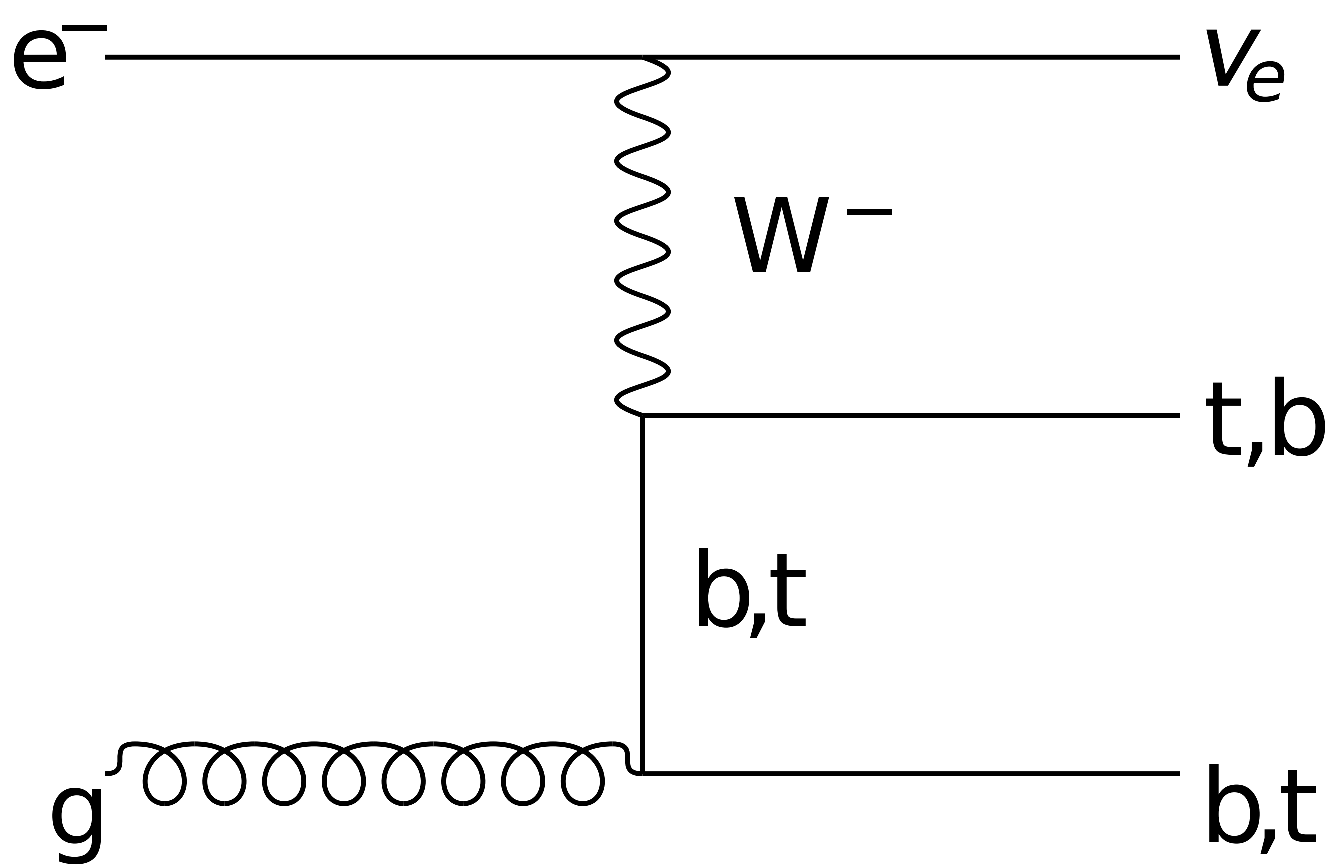

FIG. 3. Feynman diagrams for the $\nu_e bt$ background.

Benchmarks points of 2HDM-III for analysis of H+

2HDM-III like-	Parameters			$\sigma(ep \to \nu_e H^- q)$ (pb)				$\mathrm{BR}(H^- \to b\bar{c})$	$\mathrm{BR}(H^- \to \tau\bar{\nu}_\tau)$
	X	Y	Z	$m_{H^\pm} = 110$ GeV	130 GeV	150 GeV	170 GeV	$m_{H^\pm} = 110$ GeV	$m_{H^\pm} = 110$ GeV
I	0.5	17.5	0.5	2.56×10^{-2}	1.30×10^{-2}	3.47×10^{-3}	1.35×10^{-4}	9.57×10^{-1}	2.5×10^{-4}
II	20	1.5	20	2.18×10^{-2}	1.13×10^{-2}	2.95×10^{-3}	5.89×10^{-5}	9.9×10^{-1}	2.22×10^{-4}
X	0.03	1.5	-33.33	6.49×10^{-2}	3.39×10^{-2}	8.83×10^{-3}	2.34×10^{-4}	9.28×10^{-2}	9.04×10^{-1}
Y	13	1.5	$-1/13$	6.41×10^{-2}	3.27×10^{-2}	8.47×10^{-3}	2.2×10^{-4}	9.91×10^{-1}	6.12×10^{-3}

TABLE II. The BPs that we studied for the 2HDM-III in the incarnations like-I, -II, -X and -Y. We present cross sections and BRs at Parton level, for some $H^\pm$ mass choices.

- Scenario 2HDM-III like-I: $\cos(\beta-\alpha) = 0.5$, $\chi^u_{22} = 1$, $\chi^u_{23} = 0.1$, $\chi^u_{33} = 1.4$, $\chi^d_{22} = 1.8$, $\chi^d_{23} = 0.1$, $\chi^d_{33} = 1.2$, $\chi^\ell_{22} = -0.4, \chi^\ell_{23} = 0.1$, $\chi^\ell_{33} = 1$ with $Y \gg X, Z$.
- Scenario 2HDM-III like-II: $\cos(\beta-\alpha) = 0.1$, $\chi^u_{22} = 1$, $\chi^u_{23} = -0.53$, $\chi^u_{33} = 1.4$, $\chi^d_{22} = 1.8$, $\chi^d_{23} = 0.2$, $\chi^d_{33} = 1.3$, $\chi^\ell_{22} = -0.4, \chi^\ell_{23} = 0.1$, $\chi^\ell_{33} = 1$ with $X, Z \gg Y$.
- Scenario 2HDM-III like-X: the same parameters of scenario 2HDM-III like-II but $Z \gg X, Y$.
- Scenario 2HDM-III like-Y: the same parameters of scenario 2HDM-III like-II but $X \gg Y, Z$.

For light charged Higgs

$$\Gamma(H^{\pm} \to u_i d_j) = \frac{3G_F m_{H^{\pm}} (m_{d_j}^2 |X_{ij}|^2 + m_{u_i}^2 |Y_{ij}|^2)}{4\pi\sqrt{2}}$$

; the case $Y >>, X, Z$ the channel decay $H^{+} \to c\bar{b}$

$$m_c Y_{cb} = m_c Y_{23} = V_{cb} m_c \left(Y - \frac{f(Y)}{\sqrt{2}} \chi_{22}^{u} \right) - V_{tb} \frac{f(Y)}{\sqrt{2}} \sqrt{m_t m_c} \chi_{23}^{u}$$

$(H^{\pm} \to cs)$

$$m_c Y_{cs} = m_c Y_{22} = V_{cs} m_c \left(Y - \frac{f(Y)}{\sqrt{2}} \chi_{22}^{u} \right) - V_{ts} \frac{f(Y)}{\sqrt{2}} \sqrt{m_t m_c} \chi_{23}^{u}$$

$$\frac{\mathrm{BR}(H^{\pm} \to cb)}{\mathrm{BR}(H^{\pm} \to cs)} = R_{sb} \sim \frac{|V_{tb}|^2}{|V_{ts}|^2}$$

For light charged Higgs

Other case is when $X >>, Y, Z$, we get the dominants terms $m_b X_{23}$, $m_s X_{22}$:

$$m_b X_{cb} \;=\; m_b X_{23} = V_{cb} m_b \left(X - \frac{f(X)}{\sqrt{2}} \chi^d_{33} \right) - V_{cs} \frac{f(X)}{\sqrt{2}} \sqrt{m_b m_s} \chi^d_{23}$$

$$m_s X_{cs} \;=\; m_s X_{22} = V_{cs} m_s \left(X - \frac{f(X)}{\sqrt{2}} \chi^d_{22} \right) - V_{ts} \frac{f(X)}{\sqrt{2}} \sqrt{m_b m_s} \chi^d_{23}$$

If $\chi = O(1)$ and positive then $\left(X - \frac{f(X)}{\sqrt{2}} \chi^d_{33} \right)$ is small and $R_{sb} \sim \frac{|V_{cs}|^2}{|V_{cb}|^2}$,

Other situation is when, $\chi = O(1)$ and negative, then $R_{sb} \sim \frac{m_b^2 |V_{cb}|^2}{m_s^2 |V_{cb}|^2}$;

A.G. Akeroyd, S. Moretti and J. Hernández-Sánchez, PRD85:115002 (2012)

J. Hernandez-Sanchez, S. Moretti, R. Noriega-Papaqui, A. Rosado, JHEP07 (2013) 044

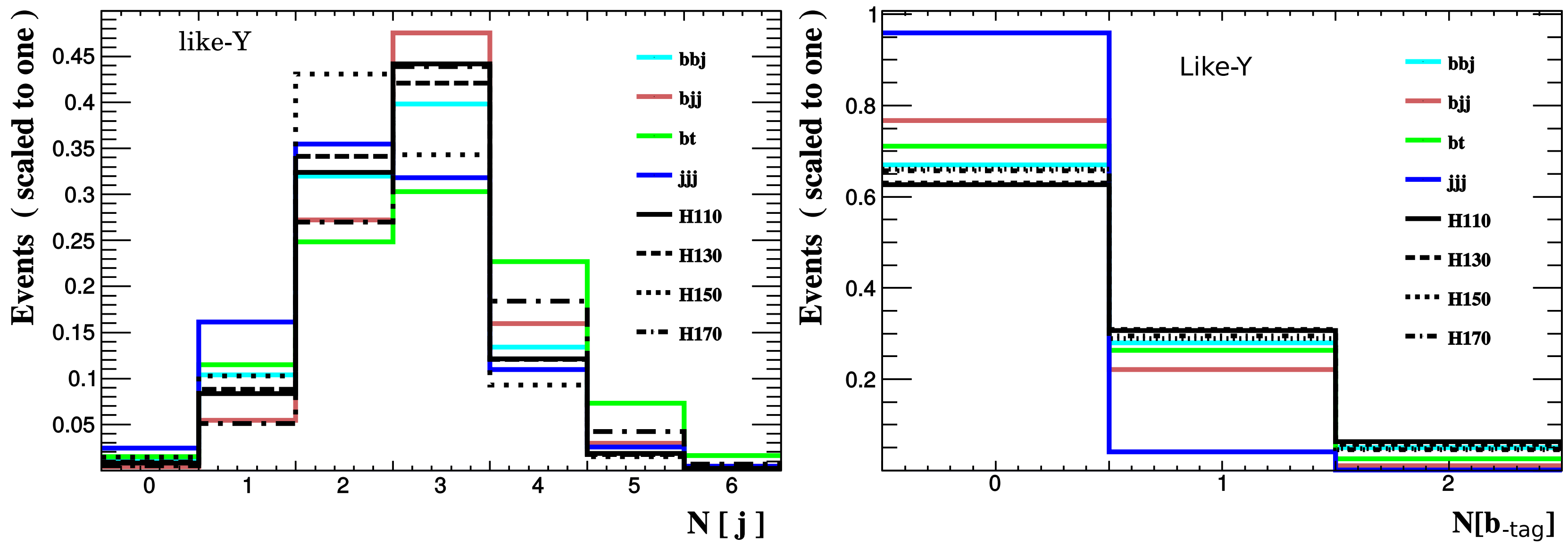

FIG. 6. Distributions for the process $e^- q \rightarrow \nu_e H^- b$ followed by $H^- \rightarrow b\bar{c}$: in the left panel we present the multiplicity of all jets while in the right panel we present the multiplicity of the b-tagged ones. The like-Y case is illustrated. The normalisation is to unity.

Cut 1: Select 3 jets

Cut 2: Select 2 jet b-tagged for H - —>cb

1 jet b-tagged for H- —>tau nu

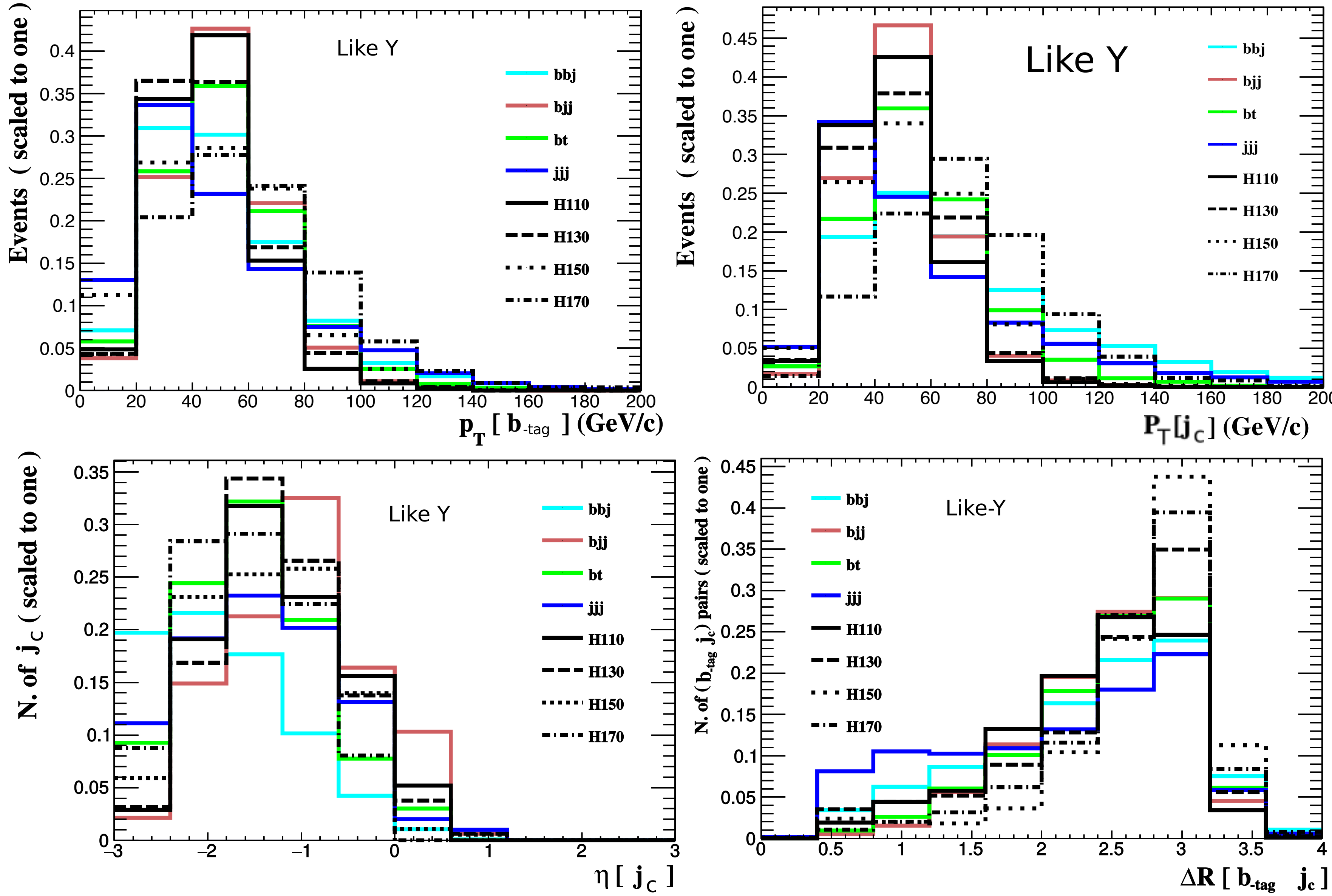

FIG. 7. Distributions for the process $e^- q \to \nu_e H^- b$ followed by $H^- \to b\bar{c}$: in the top-left panel we present the transverse momentum of the central b-tagged jet, in the top-right panel we present the transverse momentum of the central light jet, in the bottom-left panel we present the pseudorapidity of the central light jet while in the bottom-right panel we present the separation between the two central jets. The like-Y case is illustrated. The normalisation is to unity.

Cut 3: PT > 30 GeV. Cut 4 : eta<|2.5|

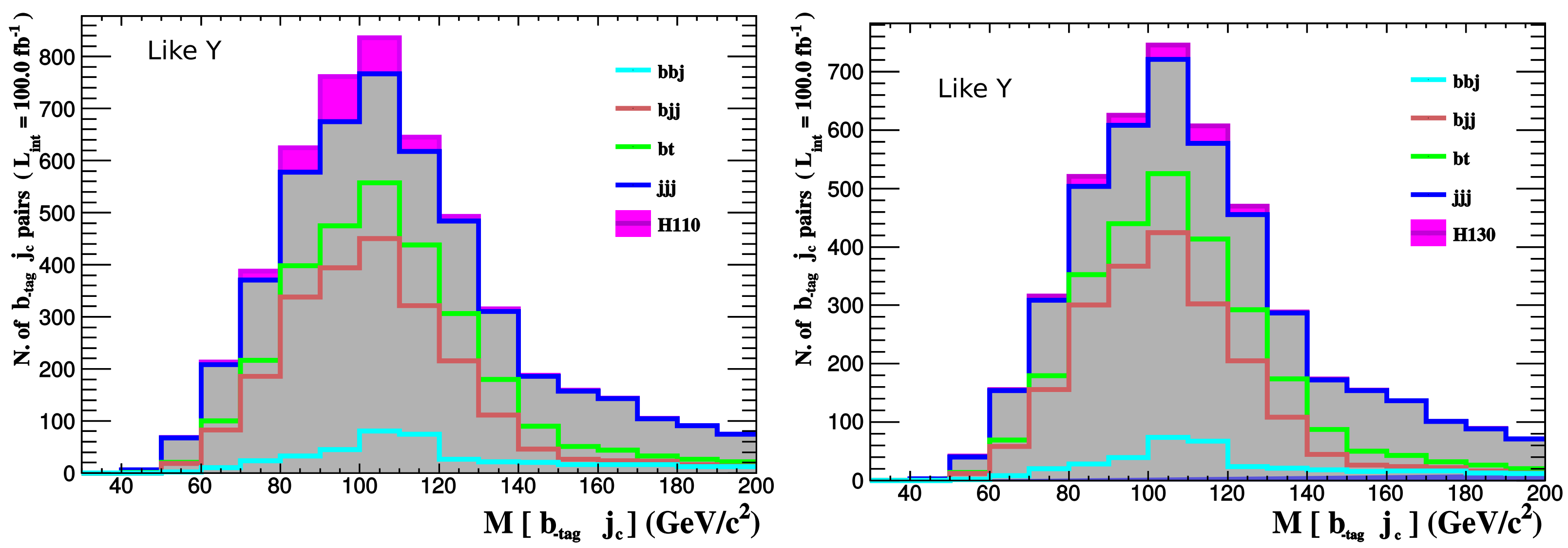

FIG. 8. Distributions for the process $e^- q \to \nu_e H^- b$ followed by $H^- \to b\bar{c}$ in the invariant mass of the two central jets for $m_{H^\pm} = 110$ GeV (left) and $m_{H^\pm} = 130$ GeV (right). The like-Y case is illustrated. The normalisation is to the total event rate for $L = 100$ fb^{-1}.

Signal	Scenario	Events (raw)	Cut I	Cut II	Cut III	Cut IV	$(\mathcal{S}/\sqrt{\mathcal{B}})_{100\ \text{fb}^{-1}(1000\ \text{fb}^{-1})[3000\ \text{fb}^{-1}]}$
$\nu_e H^\pm b$	I-110	2562	298	182	134	54	1.43 (4.52) [7.82]
	I-130	1300	139	82	64	19	0.58 (1.82) [3.16]
	I-150	347	29	13	11	3	0.16 (0.5) [0.86]
	I-170	13	1.29	0.62	0.51	0.14	0.01 (0.03) [0.05]
$\nu_e H^\pm b$	II-110	2183	245	151	122	53	1.4 (4.43) [7.68]
	II-130	1128	128	84	71	22	0.7 (2.21) [3.82]
	II-150	294	28	14	13	4	0.2 (0.65) [1.13]
	II-170	6	0.6	0.33	0.3	0.08	0.005 (0.017) [0.029]
$\nu_e H^\pm b$	Y-110	6417	468	567	347	156	4.18 (12.99) [22.5]
	Y-130	3268	366	204	156	46	1.43 (4.53) [7.84]
	Y-150	847	68	29	23	6	0.33 (1.06) [1.83]
	Y-170	22	2.3	1.12	0.89	0.25	0.017 (0.05) [0.09]
$\nu_e bbj$		20169	2011	748	569	125	$\mathcal{B} = 1441$ $\sqrt{\mathcal{B}} = 37.9$
$\nu_e bjj$		117560	10278	7211	5011	718	
$\nu_e bt$		41885	2278	1418	1130	188	
$\nu_e jjj$		867000	9238	3221	2593	409	

TABLE III. Significances obtained after the sequential cuts described in the text for the signal process $e^- q \to \nu_e H^- b$ followed by $H^- \to b\bar{c}$ for four BPs in the 2HDM-III like-I, -II and -Y. The simulation is done at detector level. In the column Scenario, the label A-110(130)[150]{170} means $m_{H^\pm} = 110(130)[150]\{170\}$ GeV in the 2HDM-III like-A, where A can be I, II and Y.

The process $e^- q \to \nu_e H^- b$ with $H^- \to \tau \bar{\nu}_\tau$ in the 2HDM-III like-X

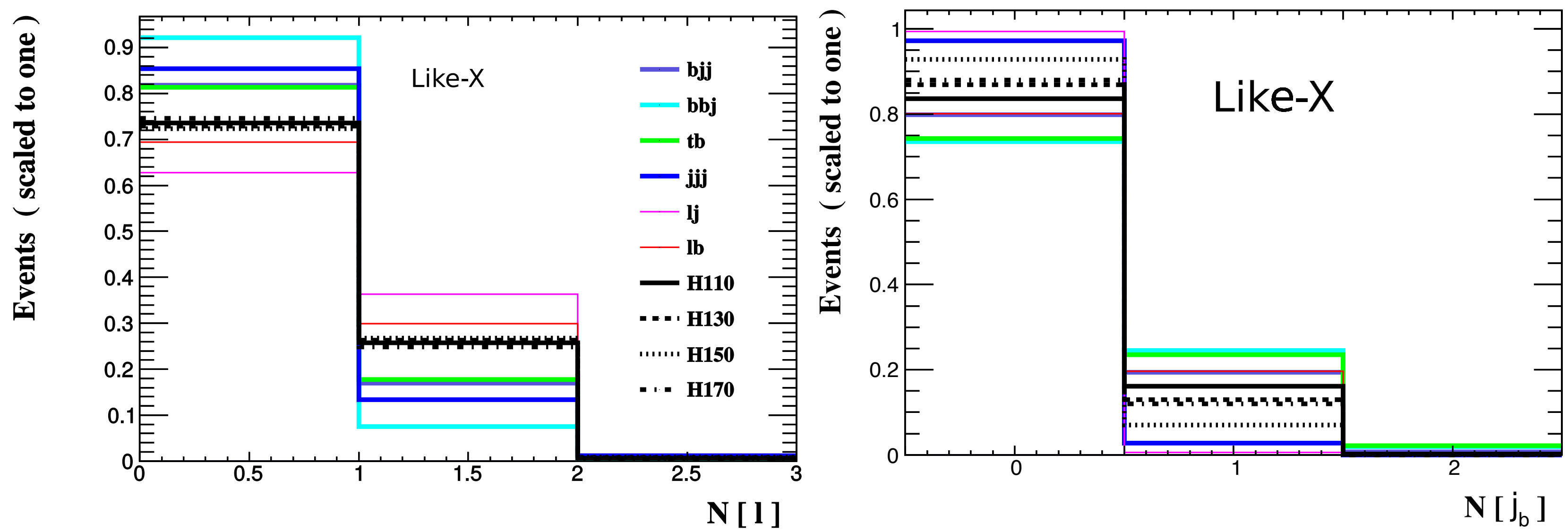

FIG. 9. Distributions for the process $e^- q \to \nu_e H^- b$ followed by $H^- \to \tau \bar{\nu}_\tau$: in the left(right) panel we present the number of leptons(b-jets) per event. The like-X case is illustrated. The normalisation is to unity.

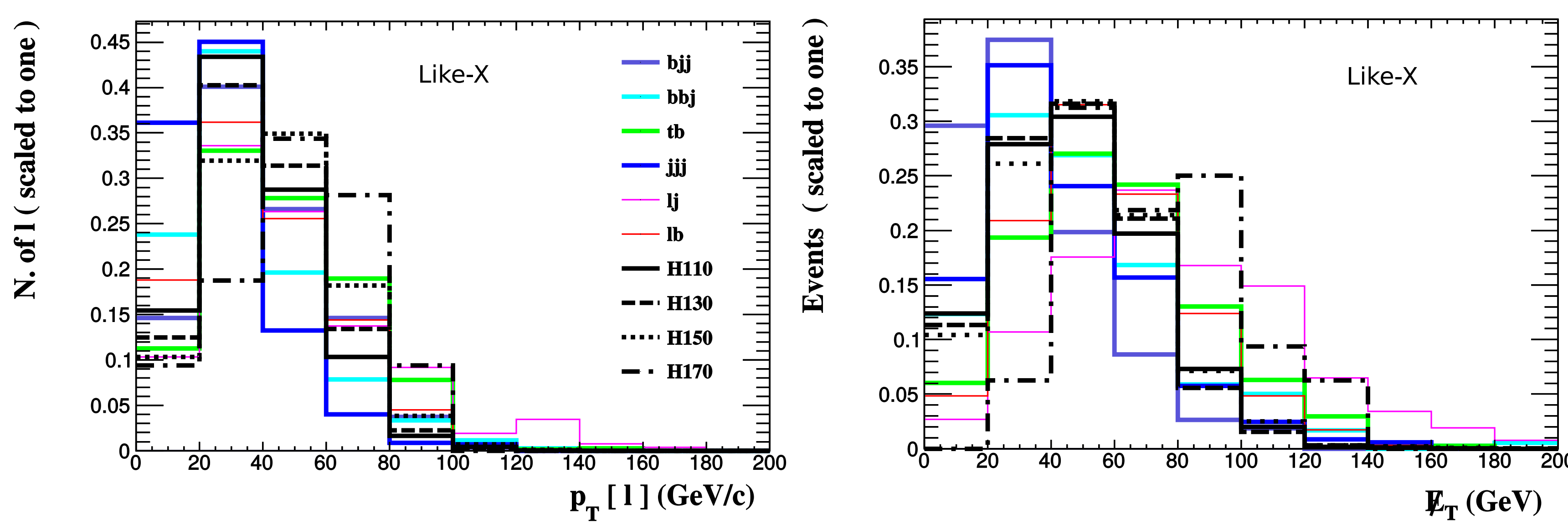

FIG. 10. Distributions for the process $e^- q \to \nu_e H^- b$ followed by $H^- \to \tau \bar{\nu}_\tau$: in the left panel we present the transverse momentum of the lepton while in the right panel we present the total missing transverse energy. The like-X case is illustrated. The normalisation is to unity.

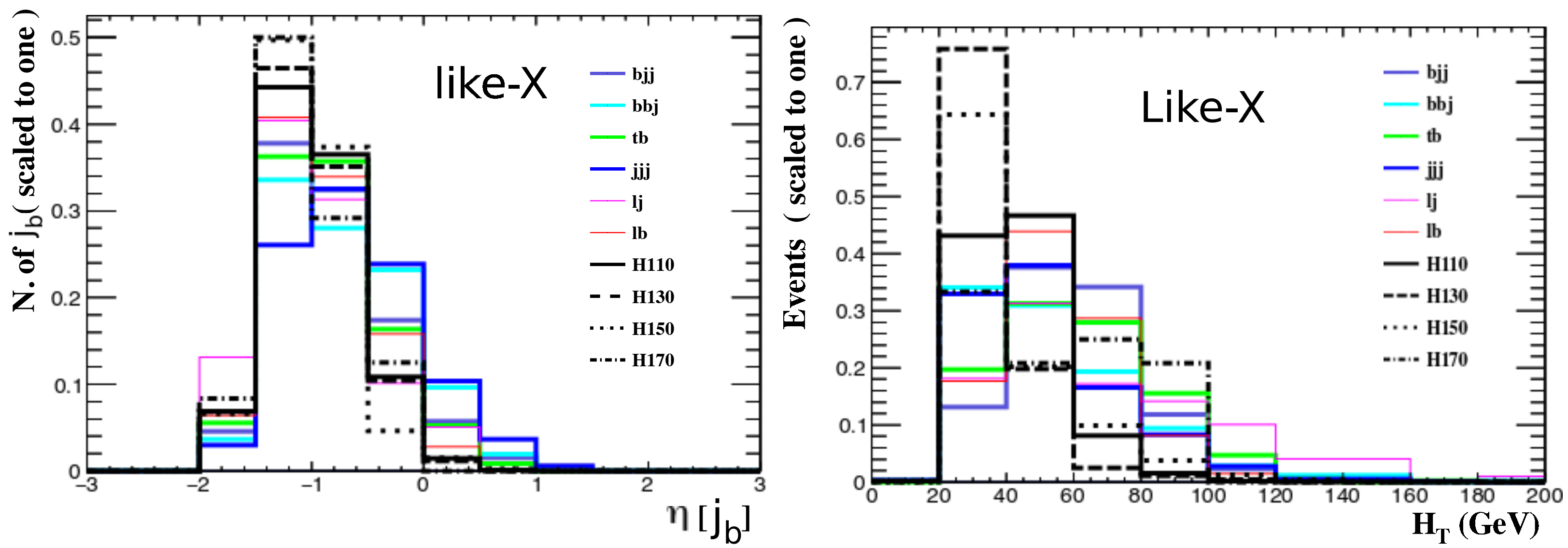

FIG. 11. Distributions for the process $e^- q \to \nu_e H^- b$ followed by $H^- \to \tau\bar{\nu}_\tau$: in the left panel we present the pseudorapidity of the b jet while in the right panel we present the total hadronic transverse energy. The like-X case is illustrated. The normalisation is to unity.

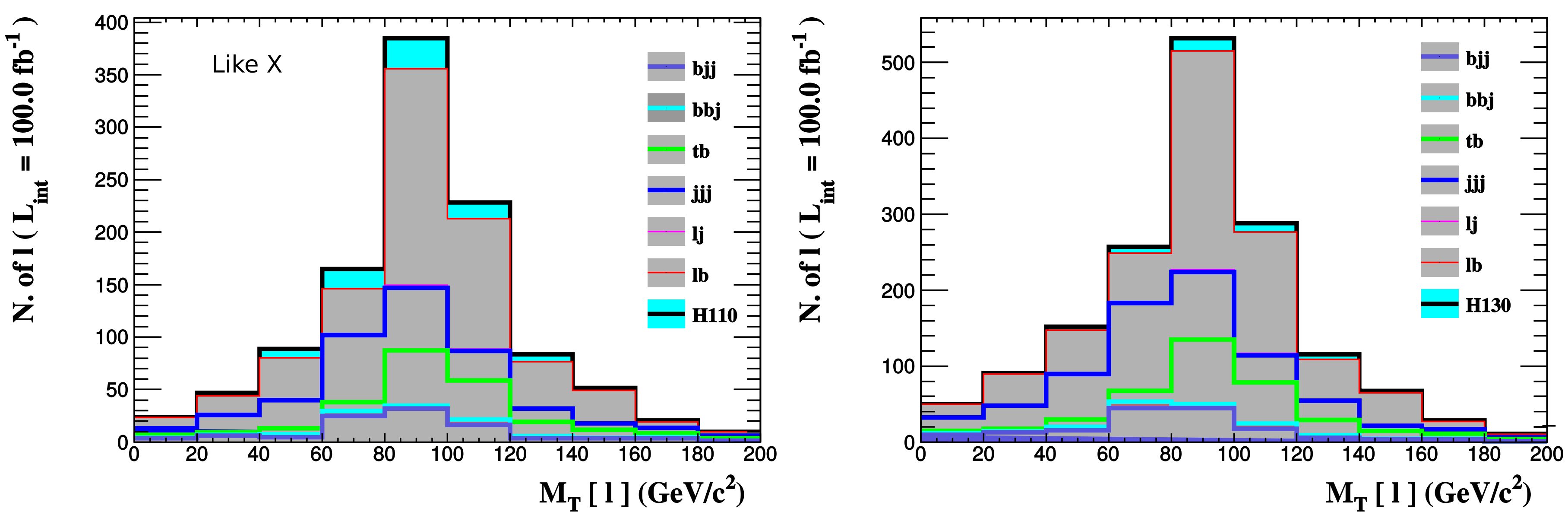

FIG. 12. Distributions for the process $e^- q \to \nu_e H^- b$ followed by $H^- \to \tau\bar{\nu}_\tau$ in the transverse mass of the final state for $m_{H^\pm} = 110$ GeV (left) and $m_{H^\pm} = 130$ GeV (right). The like-X case is illustrated. The normalisation is to the total event rate for $L = 100\ \mathrm{fb}^{-1}$.

Signal	Scenario	Events (raw)	Cut I	Cut II	Cut III	Cut IV	$(\mathcal{S}/\sqrt{\mathcal{B}})_{100\ \text{fb}^{-1}(1000\ \text{fb}^{-1})[3000\ \text{fb}^{-1}]}$
$\nu_e H^- q$	X-110	6480	178	124	94	67	2.41 (7.61) [13.19]
	X-130	3390	75	54	52	35	1.13 (3.58) [6.2]
	X-150	880	6	3	2	2	0.09 (0.29) [0.5]
	X-170	20	0.4	0.3	0.2	0.09	0.01 (0.02) [0.04]
$\nu_e bbj$		20170	85	56	23	13	$\mathcal{B} = 763$ $\sqrt{\mathcal{B}} = 27.62$
$\nu_e bjj$		117559	623	340	122	84	
$\nu_e tb$		48845	460	374	149	105	
$\nu_e jjj$		867000	981	596	267	162	
$\nu_e l \nu_l j$		23700	29	26	8	5	
$\nu_e l \nu_l b$		40400	1500	1203	569	392	

TABLE IV. Significances obtained after the sequential cuts described in the text for the signal process $e^- q \to \nu_e H^- b$ followed by $H^- \to \tau \bar{\nu}_\tau$ for four BPs in the 2HDM-III like-X. The simulation is done at detector level. In the column Scenario, the label X-110(130)[150]{170} means $m_{H^\pm} = 110(130)[150]\{170\}$ GeV in the 2HDM-III like -X.

Probing the $hc\bar{c}$ coupling at a Future Circular Collider in the electron-hadron mode

Point	$X(Z)$	Y	BR($\phi^0 \to ab$)	$\sigma(e^- p \to e^- \phi^0 q)$	Events (1 ab^{-1})
Ia	0.5(0.5)	6.5	BR($h \to b\bar{b}$) = 0.513	0.875 pb	2×10^5
	$\mu = 0.88$		BR($h \to c\bar{c}$) = 0.484		2×10^4
	$\kappa_c = 1.5$		BR($h \to sb$) = 1.99×10^{-3}		52
			BR($h \to s\bar{s}$) = 8.18×10^{-9}		0
IIa	1(1)	4	BR($h \to b\bar{b}$) = 0.67	0.958 pb	2×10^5
	$\mu = 1.16$		BR($h \to c\bar{c}$) = 0.23		2×10^4
	$\kappa_c = 2$		BR($h \to sb$) = 0.093		1×10^3
			BR($h \to s\bar{s}$) = 2.87×10^{-3}		7
Y-min	5(-1/5)	5	BR($h \to b\bar{b}$) = 0.498	1.08 pb	2×10^5
	$\mu = 0.86$		BR($h \to c\bar{c}$) = 0.289		2×10^4
	$\kappa_c = 1.7$		BR($h \to sb$) = 0.21		7×10^3
			BR($h \to s\bar{s}$) = 1.96×10^{-3}		5

TABLE III. Relevant cross sections, BRs and event rates (for the machine configuration given in the previous figure caption) for our scenarios Ia, IIa and Y, each mapped in terms of X, Y and Z values. We have included the allowed values for μ and κ_c for each BPs. Here, we have included the following tagging efficiencies in the last column: $\epsilon_b = 0.6$, $\epsilon_c = 0.24$ and $\epsilon_s = 0.05$ [78].

J. Hernandez-Sanchez, C.G. Honorato, Stefano Moretti
Arxiv: 2108.05448, submitted to EJPC.

Background	Cross section [pb]	Number of events
$\nu_e jjj$	172	1.75×10^8
$\nu_e bjj$	16.1	1.61×10^7
$\nu_e bbj$	1.8	1.8×10^6
$\sum \nu 3j$	189.9	10^8
$\nu_e llj$	3.09	3.09×10^6
$\nu_e tb$	12.47	1.24×10^7
$ejjj$	948	9.48×10^8
$ebjj$	17.8	1.78×10^7
$ebbj$	75.4	75.4×10^7
$\sum ejjj$	1040	10^9
ett	0.35	3.5×10^5

TABLE V. Background cross sections and event rates at parton level after the following cuts: $p_T(q) > 10$ GeV, $\Delta R(q,q) > 0.3$ and $|\eta(q)| < 7$ (assuming the usual FCC-eh parameters).

the effective di-jet final state defined above as $N_j + N_{b\to j} + N_{c\to j}$

Signal	Raw events	Sim Events	Set **A)**	Set **B)**	Set **C)**	Set **D)**	Set **E)**	Significance
Ia	875000	890530	633866 36075	190986 10869	91117 5186	77079 4387	36054 2052	36.3 8.31
IIa	958000	970336	609152 32350	178088 9457	87714 4658	72312 3840	30898 1641	31.19 6.67
Y	1070000	1085244	736138 41941	208665 11884	101427 5776	83083 4732	35824 2040	36.08 8.27
$\Sigma\nu 3j$	1.89×10^8	19956113	176368197 10334771	40956844 2399977	9327890 546593	4960087 290650	820718 48092	$\Sigma\ B =$ 950207 58865
νtb	1.24×10^7	1254485	7880059 501285	1505048 95743	759201 48296	548492 34892	123961 7886	
$\Sigma e3j$	10^9	104495242	73393857 52792574	3093729 2225334	29137 20958	24770 17817	2750 1978	
ett	350000	353583	26046 14764	380 215	109 62	77 44	21 12	
$\Sigma\nu llj$	3090000	1434318	411923 134029	117562 38253	29915 9733	19052 6199	2757 897	

TABLE VI. Cutflow for all signals and backgrounds. Here, in each cell, the top line represents the number of light di-jet events while the bottom one refers to those enriched by $c\bar{c}$ states, as described in the text.

$N_{b\to j}$. (In fact, the latter also includes a $\propto (1-\epsilon_b)$

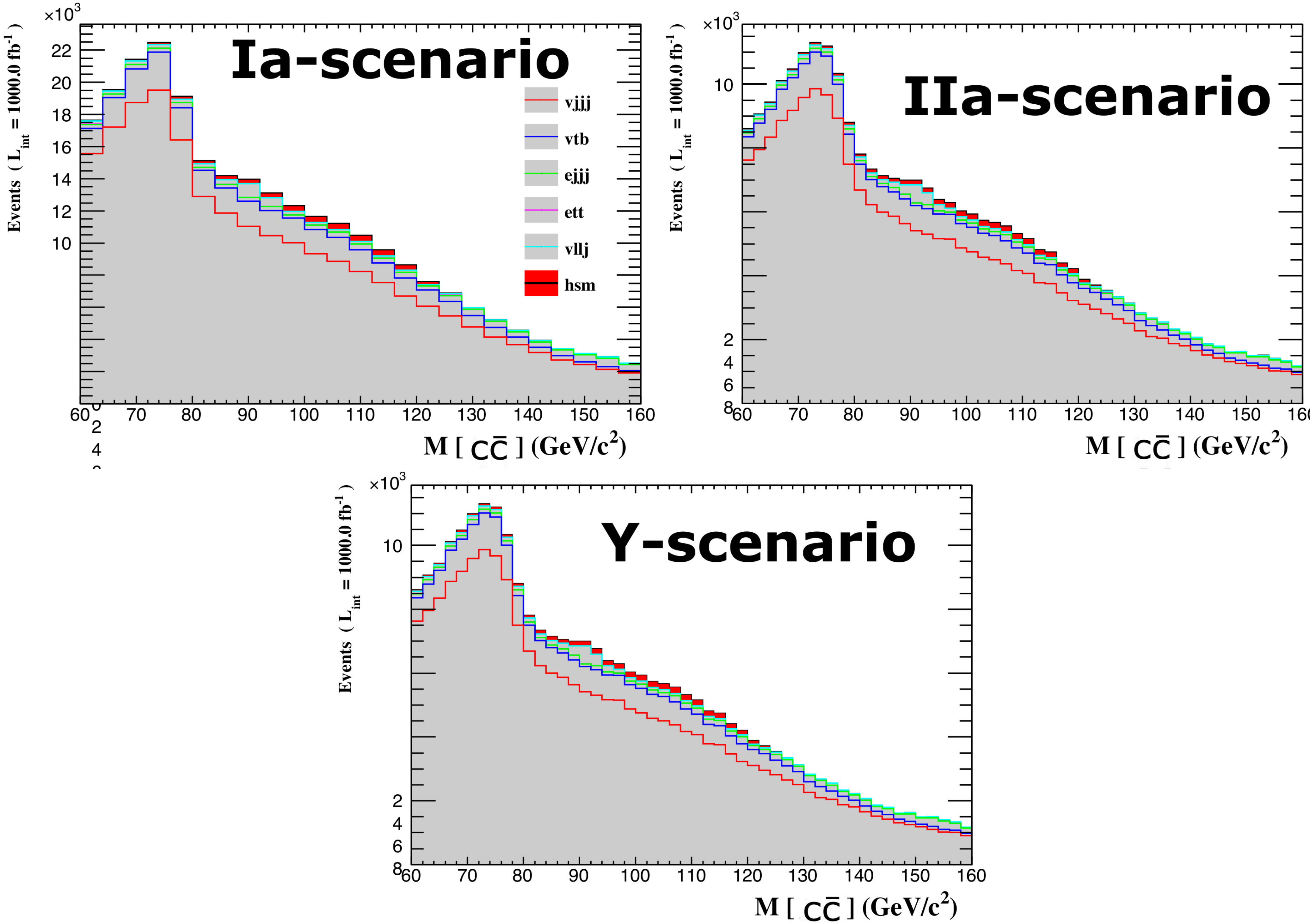

FIG. 5. Di-jet invariant mass distribution. These histograms are made for the Ia (top-left), IIa (top-right) and Y (bottom) incarnations of the 2HDM-III signal (red histogram) as well as the five categories of background discussed in the text (here stacked beneath the signal). Here, we present the rates for the case of $c\bar{c}$-tagged sample.

Summary

We show the outlook of ep colliders and how can identify new physics

We study the 2HDM-III as effective Lagrangian that induce flavor violating signatures and interesting signals like h,H —> sb.

We study the signal h,H —> sb in the future ep collider LHeC: e p —> q nu h. We have a significance up to 5 for h SM-like and for H with mass 130-150 GeV: a significance around to 4 for both colliders LHeC and FCC-eh.

Our study is consistent with flavor physics, Higgs physics and EWPO.

Following the some strategies for the neutral Higgs boson, we study the production of H+ in the channel cb for the future ep collider LHeC and extrapolate our results for FCC-eh.

We show some results for H- —>cb. We have sufficient event rates in order to get a significance 4.18 at 100 fb^-1 (6.89 at1000 fb^-1) for LHeC. For FCC-eh, the significance could reach 11.2 at 1000 fb^-1

We study the signal h —> cc in the future ep collider FCCeh.